

## The role of shelf morphology on storm-bed variability and stratigraphic architecture, Lower Cretaceous, Svalbard

STEN-ANDREAS GRUNDVÅG\* , MADSE. JELBY† , SNORRE OLAUSSEN‡ and KASIA K. ŚLIWIŃSKA§ 

\*Department of Geosciences, UiT The Arctic University of Norway, PO Box 6050 Langnes, Tromsø, N-9037, Norway (E-mail:stenndreas.grundvag@uit.no)

†Department of Geosciences and Natural Resource Management, University of Copenhagen, Øster Voldgade 10, Copenhagen K, DK-1350, Denmark

‡Department of Arctic Geology, The University Centre in Svalbard, PO Box 156, Longyearbyen, N-9171, Norway

§Geological Survey of Denmark and Greenland (GEUS), Øster Voldgade 10, Copenhagen K, DK-1350, Denmark

Associate Editor – Fabrizio Felletti

### ABSTRACT

The dominance of isotropic hummocky cross-stratification, recording deposition solely by oscillatory flows, in many ancient storm-dominated shoreface–shelf successions is enigmatic. Based on conventional sedimentological investigations, this study shows that storm deposits in three different and stratigraphically separated siliciclastic sediment wedges within the Lower Cretaceous succession in Svalbard record various depositional processes and principally contrasting sequence stratigraphic architectures. The lower wedge is characterized by low, but comparatively steeper, depositional dips than the middle and upper wedges, and records a change from storm-dominated offshore transition – lower shoreface to storm-dominated prodelta – distal delta front deposits. The occurrence of anisotropic hummocky cross-stratification sandstone beds, scour-and-fill features of possible hyperpycnal-flow origin, and wave-modified turbidites within this part of the wedge suggests that the proximity to a fluvio-deltaic system influenced the observed storm-bed variability. The mudstone-dominated part of the lower wedge records offshore shelf deposition below storm-wave base. In the middle wedge, scours, gutter casts and anisotropic hummocky cross-stratified storm beds occur in inferred distal settings in association with bathymetric steps situated across the platform break of retrogradationally stacked parasequences. These steps gave rise to localized, steeper-gradient depositional dips which promoted the generation of basinward-directed flows that occasionally scoured into the underlying seafloor. Storm-wave and tidal current interaction promoted the development and migration of large-scale, compound bedforms and smaller-scale hummocky bedforms preserved as anisotropic hummocky cross-stratification. The upper wedge consists of thick, seaward-stepping successions of isotropic hummocky cross-stratification-bearing sandstone beds attributed to progradation across a shallow, gently dipping ramp-type shelf. The associated distal facies are characterized by abundant lenticular, wave ripple cross-laminated sandstone, suggesting that the basin floor was predominantly positioned above, but near, storm-wave base. Consequently, shelf morphology and physiography, and the nature of the feeder system (for example, proximity to deltaic systems) are inferred to

exert some control on storm-bed variability and the resulting stratigraphic architecture.

**Keywords** Hummocky cross-stratification, Lower Cretaceous, storm-dominated shelf deposits, Svalbard, tempestites.

## INTRODUCTION

Sandstone storm deposits form an important part of many ancient shelf–shoreface successions and have received a considerable amount of attention in the literature for the last few decades (Dott & Bourgeois, 1982; Duke, 1985; Duke *et al.*, 1991; Cheel & Leckie, 1993; Myrow & Southard, 1996; Dumas & Arnott, 2006; Quin, 2011; Jelby *et al.*, 2020). This is mainly due to the ongoing discussion on how sand is transported across shelves during storms (Swift *et al.*, 1987; Leckie & Krystinik, 1989; Lamb *et al.*, 2008; Basilici *et al.*, 2012a; Collins *et al.*, 2017) and the origin of hummocky cross-stratification (HCS), which commonly occurs in storm deposits (Quin, 2011; Morsilli & Pomar, 2012; Jelby *et al.*, 2020). Because many ancient shelf successions are dominated by thick-bedded isotropic HCS sandstone beds, characterized by no preferred lamina dip-orientation (Fig. 1A), the first depositional models for HCS focused on the oscillatory motion of storm-waves (Harms *et al.*, 1975; Dott & Bourgeois, 1982; Southard *et al.*, 1990). Some laboratory experiments and forward modelling studies indicate that hummocky-like bedforms typically form under long-periodic waves and moderate to high oscillatory intensities with a very weak to no unidirectional-flow component (Arnott & Southard, 1990; Dumas *et al.*, 2005; Dumas & Arnott, 2006). However, in most cases the hydrodynamic requirements for thick HCS sandstone beds to accumulate will necessarily have to involve large volumes of sand brought into suspension and across the shelf by unidirectional flows followed by rapid sand deposition in concert with reworking by oscillatory flows. It has therefore been debated whether or not pure oscillatory currents are capable of transporting sand onto and across shelves. Due to the wide range of storm-bed architectures reported from the stratigraphic record (Jelby *et al.*, 2020), cross-shelf transport by geostrophic currents (Leckie & Krystinik, 1989; Duke, 1990; Midtgaard, 1996), combined-flows (Nøttvedt & Kreisa, 1987; Dumas *et al.*, 2005; Quin, 2011) and storm surges (Mount,

1982), as well as various density-driven and wave-enhanced gravity flows (Myrow *et al.*, 2002; Lamb *et al.*, 2008), have all gained support. Although a combination of these processes most likely governs deposition during most storms, the dominance of isotropic HCS sandstones reported in many ancient shelf–shoreface successions remains enigmatic (Brenchley *et al.*, 1993). Facies models for ancient storm-dominated shelves show that HCS sandstone beds are common in transgressive shelf sheets and offshore bars in mid-shelf settings (Bourgeois, 1980) or in regressive shoreline tongues on the innermost shelf (Aigner & Reineck, 1982; Brenchley *et al.*, 1993; Taylor & Lovell, 1995; Midtgaard, 1996; Hampson & Storms, 2003). In addition, HCS commonly occurs in shelf-edge delta successions, because storm-waves directly impact these shorelines without being dampened (Carvajal & Steel, 2009; Bowman & Johnson, 2014; Peng *et al.*, 2016).

Hummocky cross-stratification is generally regarded to result from the combined migration and aggradation of three-dimensional bedforms (Quin, 2011) operating in the zone between the storm-wave base (SWB) and fair-weather wave base (FWWB). In nearshore areas, isotropic HCS typically grades shoreward into: (i) anisotropic HCS characterized by a preferred lamina dip-orientation (Fig. 1B); (ii) swaley cross-stratification characterized by a predominance of concave-up lamina depressions (swales); and (iii) eventually plane-parallel stratification (Aigner & Reineck, 1982; Dumas & Arnott, 2006). Some of the classic facies models for storm-dominated shoreface–shelf systems generally depict a distally-deepening environment where suspension settling and density-driven turbidity flows dominate offshore below SWB (Harms *et al.*, 1975; Aigner & Reineck, 1982; Dott & Bourgeois, 1982; Walker, 1984). These processes deposit finely laminated mudstones interbedded with thin-bedded turbidites (i.e. ‘graded rhythmites’) (Reineck & Singh, 1972). Although these models are valid for distally deepening shelves with moderate to steep gradients, they do not take into account the gently sloping nature and

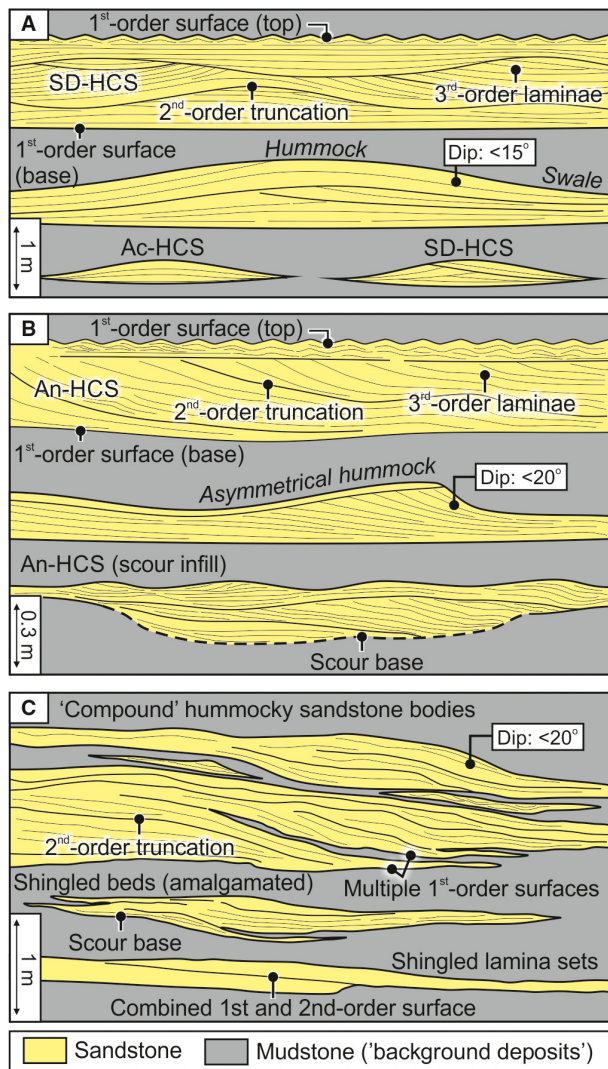


**Fig. 1.** Conceptual line drawings of isotropic and anisotropic hummocky cross-stratification (HCS), based on field observations. (A) Different configurations of isotropic HCS, which is characterized by no preferred lamina dip-orientation and occurs as scour-and-drape (SD) or accretionary (Ac) HCS (*sensu* Cheel & Leckie, 1993). (B) Different configurations of anisotropic (An) HCS, which is characterized by preferred lamina dip-orientation and occurs in tabular to wedge-shaped beds, or as infills of scour. (C) Anisotropy is also observed as laterally or frontally accreted beds within 'compound' hummocky sandstone bodies (*sensu* Midtgaard, 1996; cf. Jelby *et al.*, 2020). Bounding surface-terminology is adopted from Dott & Bourgeois (1982).

shallow water depths of many ancient ramp-type shelves typical of epeiric seas where the role of offshore-directed, gravity-driven flows is reduced (Jelby *et al.*, 2020). Instead, epeiric seas

are characterized by frequent storm-wave reworking of deposited sediment, even in shelf settings located several hundred kilometres from the shore, as evidenced by the presence of laterally extensive sandstone sheets dominated by isotropic HCS in some ancient examples (Brenchley *et al.*, 1986, 1993; Runkel *et al.*, 2007; Jelby *et al.*, 2020). Thus, shelf morphology and physiography appear to impose a strong control on storm-bed variability, which is inherently related to the stratigraphic architecture of the resulting storm-dominated shoreface-shelf succession.

In order to investigate the relationship between these factors, three Lower Cretaceous storm-dominated, HCS-bearing, siliciclastic shelf successions in Svalbard, Arctic Norway (Fig. 2A), are compared and contrasted. Each of the successions consists of shallow-marine sandstone-dominated units that interfinger with and apparently pass basinward into offshore mudstone units. As such, the sandstone units represent basinward-thinning sediment wedges, herein referred to as the upper, middle and lower wedges (Figs 2D and 3). Internally, the wedges comprise progradational to retrogradational parasequence sets (*sensu* Van Wagoner *et al.*, 1990), and they accumulated under principally different hydrodynamic conditions. This is reflected in the facies variability of both storm beds and sequence stratigraphy between the wedges (Figs 2D, 3 and 4). Because of their extensive regional distribution and limited lateral facies variations, the wedges have been attributed to deposition on a low-gradient, ramp-type shelf (Fig. 4; Nagy, 1970; Dypvik *et al.*, 1991a; Midtkandal & Nystuen, 2009; Jelby *et al.*, 2020).

Of particular interest to this study, is the upper wedge which is dominated by isotropic HCS sandstones (Grundvåg *et al.*, 2015; Hurum *et al.*, 2016). Thus, the primary objective of this paper is to describe and interpret the stratigraphic distribution and variability of various storm-emplaced sandstone beds related to the upper wedge (Figs 2D and 3). In order to elucidate how shelf morphology (for example, steep versus gentle slopes) and physiography may influence storm-bed variability and stratigraphic architecture (for example, seaward-stepping versus landward-stepping wedges), the investigated storm beds in the upper wedge are compared with storm beds occurring in two older wedges. The middle wedge developed during regional

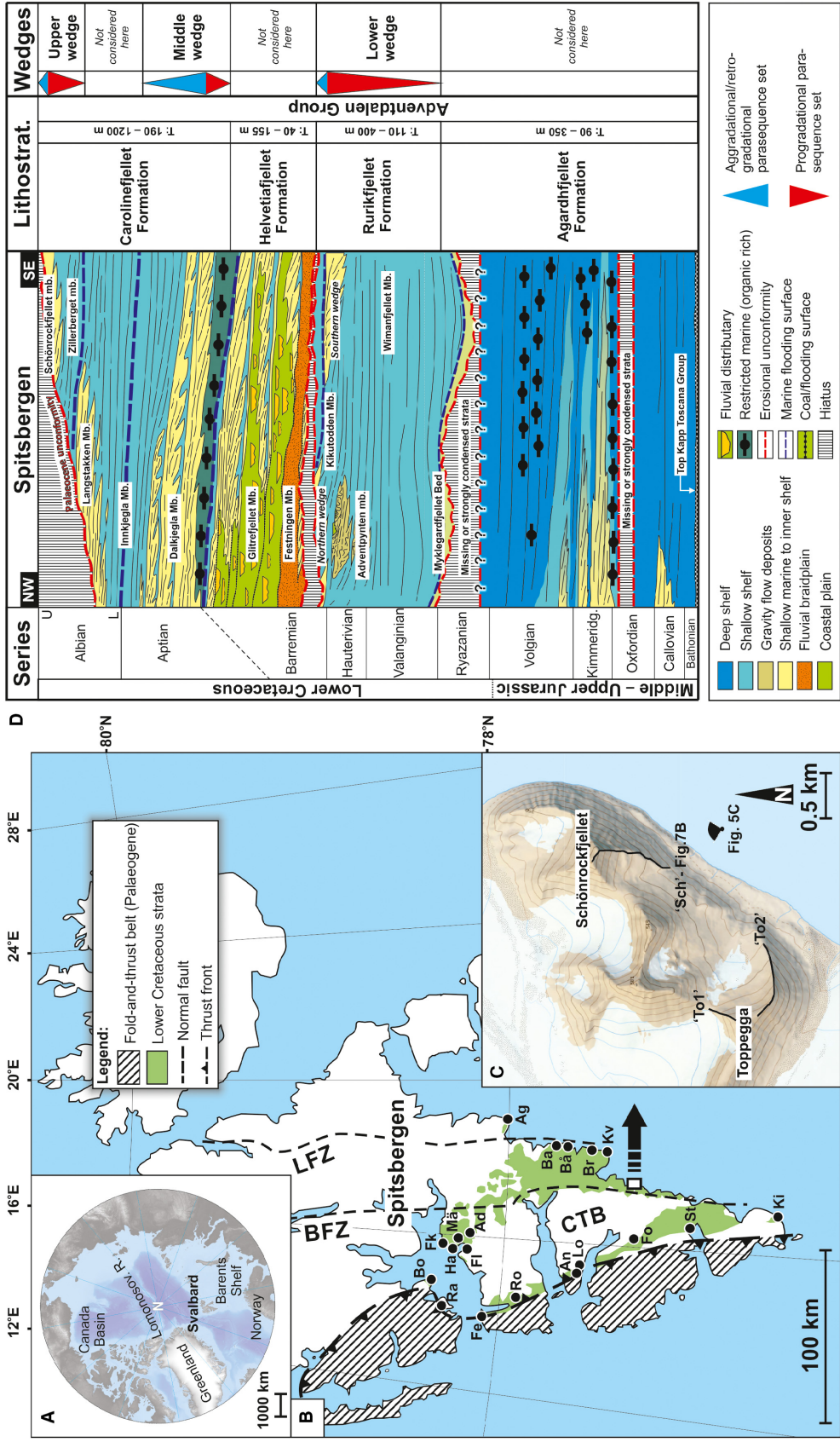


**Fig. 2.** (A) Map of the Arctic showing the position of Svalbard on the north-western corner of the Barents Shelf. N: North Pole. (B) Map of Spitsbergen showing the distribution of Lower Cretaceous strata (green) flanking the Central Tertiary Basin (CTB). Black circles indicate the location of measured sections used in this study. Ad: Adventdalen, An: Annaberget, Ag: Agardhaksla, Ba: Baugen, Bo: Bohemanflya, Br: Baronfjella, Ma: Båtsmannen, Fe: Festningen, Fl: Flyplassveien, Fk: Forkastningsfjellet, Fo: Fotografryggen, Ha: Hanaskogdalen, Ki: Kikutodden, Kv: Kvalvågen, Lo: Louiseberget, Ma: Mälardalen, Ra: Ramfjellet, Ro: Romnæstoppen, St: Strykejernet. (C) Inset map showing the location of the main study area of the upper wedge in south-eastern Spitsbergen, with black lines indicating the measured sections at Schönrockfjellet (Sch) and Toppegga (To1 and To2). Sedimentary logs are shown in Figs 7 and 8. The map is modified from TopoSvalbard (<http://toposvalbard.npolar.no>). (D) Lithostratigraphic chart of the Middle Jurassic to Lower Cretaceous Adventdalen Group on Spitsbergen from the north-west to south-east, showing the stratigraphic position of the investigated wedges. The chart is based on Grundvåg *et al.* (2017, 2019). Mb.: Member (formal unit), mb.: member (informal unit).

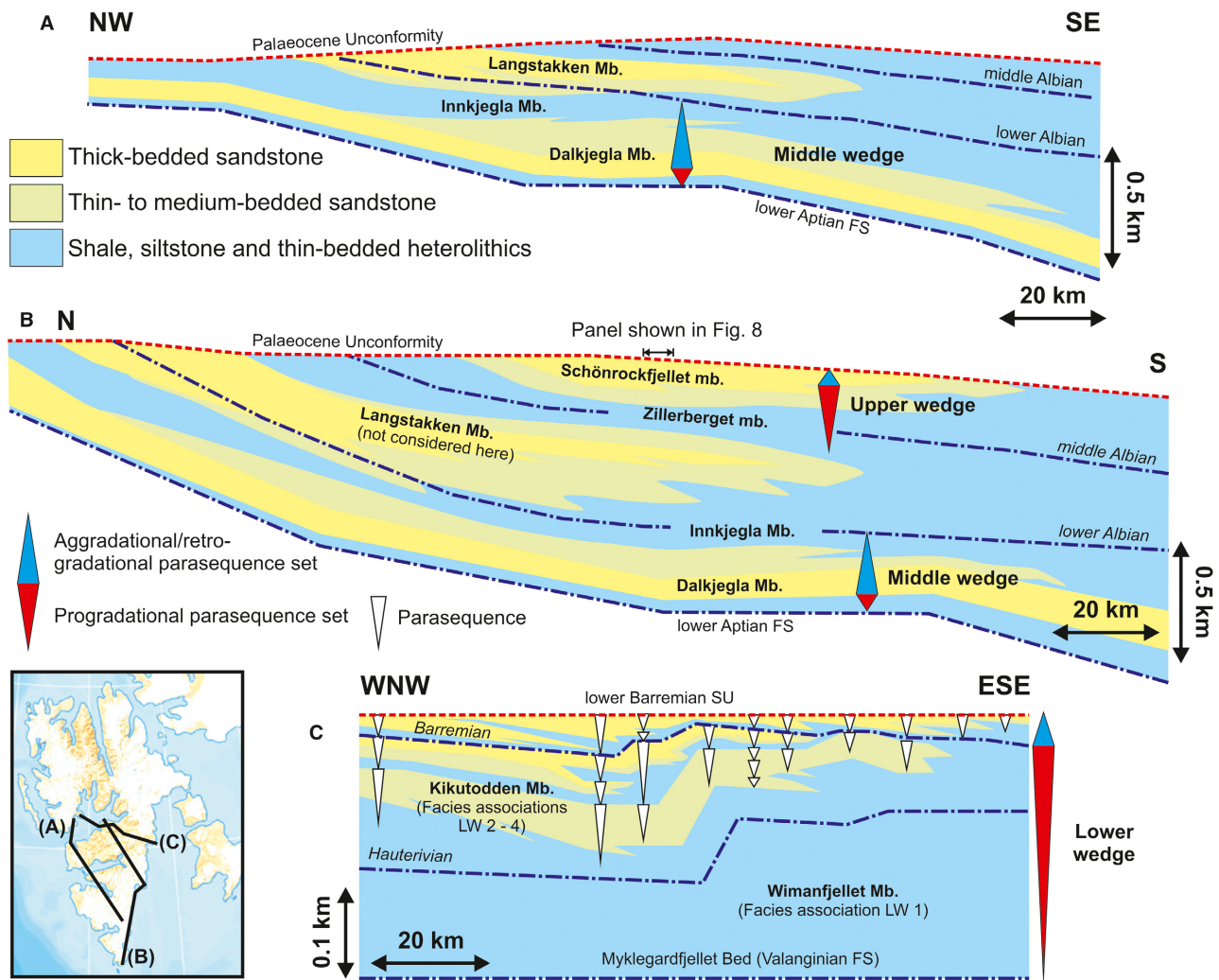


**Fig. 3.** Stratigraphic cross-sections of the Carolinefjellet and Rurikfjellet Formations across Spitsbergen. (A) North-west to south-east-oriented cross-section of the Carolinefjellet Formation in the western and northern part of the outcrop belt showing the lateral extent of the middle wedge (that is the Dalkjegla Member) and how the Palaeocene unconformity erodes the upper part of the formation. Note that the Langstakken Member is not dealt with here. (B) North to south-oriented cross-section of the Carolinefjellet Formation showing how the formation thickens southward and how the upper wedge (that is the Zillerberget and Schönrockfjellet members) only occurs locally in eastern Spitsbergen. Panels in (A) and (B) are based on regional correlation work by Nagy (1970). (C) WSE–ESE-oriented cross-section of the lower wedge (that is the Rurikfjellet Formation) demonstrating how the sandstone-bearing Kikutodden Member in the upper part of the formation thins towards the east. Based on Dypvik *et al.* (1991a), Grundvåg *et al.* (2019) and Jelby *et al.* (2020). FS: flooding surface, Mb.: Member (formal unit), mb.: member (informal unit), SU: subaerial unconformity.

transgression, and the lower wedge developed as early sedimentary response to a tectonically-induced regression (Figs 2D and 4).

### Terminology

In this paper, HCS is classified as either *isotropic* or *anisotropic* (*sensu* Cheel & Leckie, 1993; Fig. 1). Traditionally, isotropic HCS has been sub-divided into: (i) *accretionary*; and (ii) *scour-and-drape* HCS

(*sensu* Cheel & Leckie, 1993; Fig. 1A). Although both types are recognized in this study, they commonly represent a continuum of configurations within a single bed. Thus, the term ‘isotropic’ is applied here more generally, encompassing all HCS characterized by gently dipping (<15°) and curved to undulating cross-stratification with no preferred dip-orientation (Fig. 1A).

Even though anisotropic HCS has been described in various contributions (Nøttvedt &

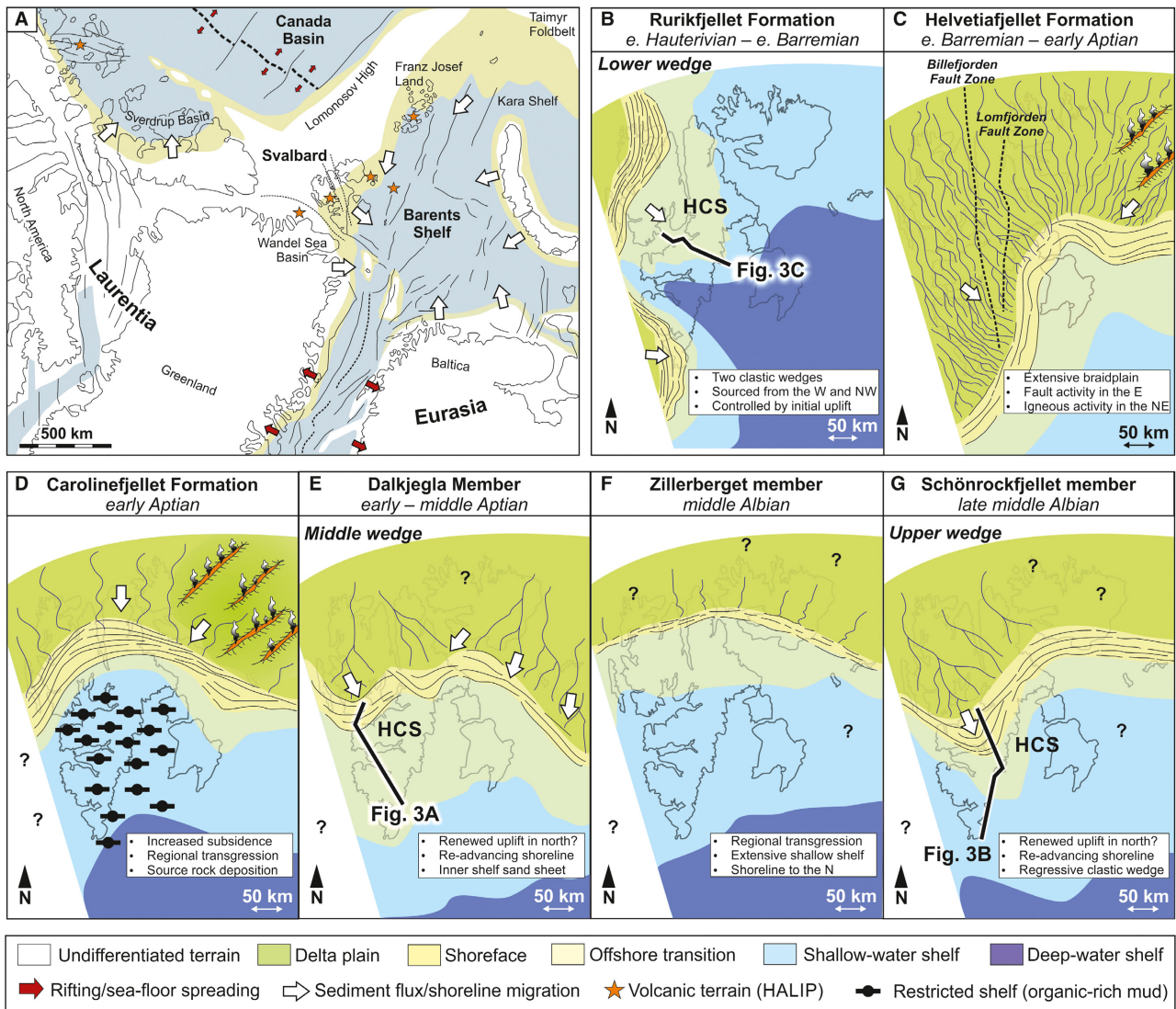


**Fig. 4.** Geological setting for Svalbard during the Early Cretaceous (A) Barremian regional reconstruction showing the location of Svalbard and the epicontinental character of the Barents Shelf. Orange stars indicate areas where Early Cretaceous igneous activity has been recorded. Red arrows indicate rifting and sea-floor spreading. The map is based on Steel & Worsley (1984) Dypvik *et al.* (2002), Torsvik *et al.* (2012), Grundvåg *et al.* (2017) and Olaussen *et al.* (2018). (B) to (G) Palaeogeographic reconstruction of Svalbard during the Early Cretaceous (early Hauterivian – late middle Albian). Hummocky cross-stratified (HCS) sandstone storm deposits occur in several stratigraphic units, indicating that storm-dominated epicontinental shelf conditions were common through the Early Cretaceous (see text for more details). Highlighted black lines in (B), (E) and (G) indicate the position of the regional panels shown in figure. The reconstructions are based on Steel & Worsley (1984), Dypvik *et al.* (1991b), Midtkandal & Nystuen (2009), Grundvåg *et al.* (2017, 2019), Olaussen *et al.* (2018) and this study.

Kreisa, 1987; Arnott & Southard, 1990; Myrow, 1992; Martel & Gibling, 1994; Midtgaard, 1996), no unequivocal definition or clear recognition criteria exist. As a result, the term has been applied to sedimentary structures of variable scales originating from different formative processes. Here, 'anisotropic HCS' is applied to all low-angle (<15°), tangential cross-stratification

with a preferred unimodal dip direction (*sensu* Cheel & Leckie, 1993). Anisotropic HCS is restricted to single sets within tabular and symmetrical to asymmetrical, lenticular-shaped beds, or as scour infills (Fig. 1B). Although not included in the definition herein, anisotropy is also observed as shingled, gently-dipping, lamina sets and lenticular-shaped storm beds, and

as frontal (or possibly lateral) accretion of sigmoidal-shaped storm beds bounded by second-order truncation surfaces (*sensu* Dott & Bourgeois, 1982) within ‘compound’ hummocky sandstone bodies (Fig. 1C; cf. Jelby *et al.*, 2020).

## GEOLOGICAL SETTING

### Tectonic framework

The Svalbard archipelago represents the uplifted and exposed north-western corner of the Barents Shelf (Fig. 2A). Lower Cretaceous strata are exposed along the margins of the SSE–NNW-trending Central Tertiary Basin (Fig. 2B). During the Early Cretaceous, Svalbard was located at 63–66°N (Shephard *et al.*, 2013), being part of a larger epicontinental basin (Fig. 4A; Steel & Worsley, 1984; Shipilov, 2008; Midtkandal *et al.*, 2019). The basin had an epicontinental character since before the breakup of Pangaea, but was fragmented with the breakup of the Lomonsov High and the opening of the Atlantic Ocean in the Cenozoic (Shipilov, 2008; Midtkandal *et al.*, 2019). During the Early Cretaceous, sediments derived from uplifted terranes bordering Svalbard did not encounter any abrupt basin deepening in the form of a shelf break. Instead, sediments were distributed by shelf processes across a regionally extensive, low-angle platform area (Fig. 4A; Midtkandal & Nystuen, 2009; Midtkandal *et al.*, 2019). Although a series of accretionary shelf-breaks have been documented in the subsurface some 300 km south of Svalbard (Marin *et al.*, 2016; Grundvåg *et al.*, 2017; Midtkandal *et al.*, 2019), these did not influence the facies development of the investigated wedges. Thermal subsidence largely controlled the regional tectonostratigraphic development of the basin. However, the Hauterivian to Aptian opening of the Canada Basin (Fig. 4A; Grantz *et al.*, 2011) caused southward tilting of the Svalbard platform in the earliest Barremian (Fig. 4C and D). Associated igneous activity peaked in the early Aptian with development of the High Arctic Large Igneous Province (HALIP; Maher, 2001; Corfu *et al.*, 2013; Senger *et al.*, 2014).

### Lithostratigraphy of the wedges

The three wedges selected for this study belong to the *ca* 1500 m thick Middle Jurassic – Lower Cretaceous Adventdalen Group (Fig. 2D; Mørk

*et al.*, 1999). The Lower Cretaceous part of the group comprises Valanginian to middle Albian strata.

The lower wedge is assigned to the Valanginian – lower Barremian Rurikfjellet Formation, which consists of the shale-dominated Wimanfjellet Member and the overlying sandstone-rich Kikutodden Member (Figs 2D, 3C, 5A, 6A and 6B; Dypvik *et al.*, 1991b; Grundvåg *et al.*, 2017, 2019; Jelby *et al.*, 2020; Śliwińska *et al.*, 2020). The two units form a 200 to 300 m thick coarsening-upward succession, with only the sandstone beds of the Kikutodden Member displaying basinward thinning (to the south-east; Fig. 3C). The succession accumulated following a Valanginian flooding event (marked FS in Fig. 3C), and represents early sedimentary response to northern uplift of Svalbard. Regionally, the Rurikfjellet Formation comprises two laterally equivalent shallow marine sandstone wedges both assigned to the Kikutodden Member (Fig. 4B; Grundvåg & Olausen, 2017; Grundvåg *et al.*, 2017; Jelby *et al.*, 2020). Only the northern wedge is dealt with here. The regional uplift culminated in the Barremian to early Aptian by deposition of the paralic Helvetiafjellet Formation (Figs 2D, 2C and 6A; Gjelberg & Steel, 1995; Midtkandal & Nystuen, 2009; Grundvåg *et al.*, 2017, 2019).

The middle wedge is assigned to the Aptian Dalkjegla and Innkjegla members of the Carlinefjellet Formation (Figs 2D, 3, 5B and 6B; Århus, 1991; Mørk *et al.*, 1999; Grundvåg *et al.*, 2017). The base of the wedge is defined by a lower Aptian shale unit deposited during a regional flooding of the Helvetiafjellet Formation coastal plain (marked FS in Figs 2D, 3A, 5B, 6A, 6B and 6F; Midtkandal *et al.*, 2016; Grundvåg *et al.*, 2017, 2019). The succeeding sandstone-dominated part of the Dalkjegla Member contains some spectacular examples of anisotropic HCS (Nøttvedt & Kreisa, 1987). The transitionally overlying Innkjegla Member is shale-dominated and marks a gradual upward-finishing of the middle wedge (Figs 2D, 3, 6A, 6G and 6H).

The upper wedge is assigned to the informally defined middle Albian Zillerberget and Schönrockfjellet members in the uppermost part of the Carlinefjellet Formation (Fig. 2D). The fine-grained and heterolithic Zillerberget member is gradationally overlain by the sandstone-dominated Schönrockfjellet member, and together the two members form a several hundred metres thick upward-coarsening succession (Figs 2D, 3B, 5C and 7A; Grundvåg *et al.*, 2015; Hurum *et al.*, 2016).

## DATA AND METHODS

The main study area is confined to the mountains of Schönrockfjellet and Toppegga in Torell Land on the south-east coast of Spitsbergen, the largest island of the Svalbard archipelago, where the upper wedge is most exposed (Fig. 2B and C). This wedge has a very limited lateral extent, being preserved within an area of *ca* 1000 km<sup>2</sup> (Fig. 3B; Nagy, 1970). One sedimentological log was retrieved from Schönrockfjellet (Sch), and two sedimentological logs were retrieved from Toppegga (To1 and To2; Figs 2C, 7 and 8). The logs comprise a cumulative thickness of 400 m measured bed-by-bed at centimetre-scale, and include descriptions of rock type, grain size, sorting, sedimentary structures, body fossils, trace fossils and bioturbation, and palaeocurrent data. The main section (Sch) was measured along the southern ridge of Schönrockfjellet (Figs 5C and 7) where Nagy (1970), Århus (1991) and Hurum *et al.* (2016) have previously conducted stratigraphic investigations (a composite section based on these studies is shown in Fig. 7A). The middle and the lower wedges are distributed across large parts of the Lower Cretaceous outcrop belt on Spitsbergen with minimum preserved extents of *ca* 13 000 km<sup>2</sup> and *ca* 8000 km<sup>2</sup>, respectively. Sedimentological data from these wedges are based on several outcrop sections across the entire outcrop belt, and onshore drill cores from Adventdalen (Figs 2B and 3; see also Grundvåg *et al.*, 2017, 2019; Jelby *et al.*, 2020). Although the upper wedge only occurs in eastern Spitsbergen (Figs 2 and 3B; Nagy, 1970), outcrops at the scale of entire mountain sides (>1.0 km laterally and >0.5 km vertically; Figs 5C and 7A) and the generally excellent outcrop quality allows precise lateral correlation and thicker measured sections than the other wedges.

## RESULTS

### Previous studies and rationale for choosing the three wedges

The investigated siliciclastic sediment wedges were mainly chosen on the basis of their well-known biostratigraphic and lithostratigraphic framework and their excellent exposures (for example, Figs 2D, 3 and 5; Nagy, 1970; Dypvik *et al.*, 1991a; Hurum *et al.*, 2016; Grundvåg *et al.*, 2017; Śliwińska *et al.*, 2020; Jelby *et al.*, 2020). In addition, the Early Cretaceous tectonic

and palaeogeographic evolution of the shelf on which the wedges accumulated, is well-constrained (Fig. 4; Grundvåg *et al.*, 2017; Olausen *et al.*, 2018; Midtkandal *et al.*, 2019).

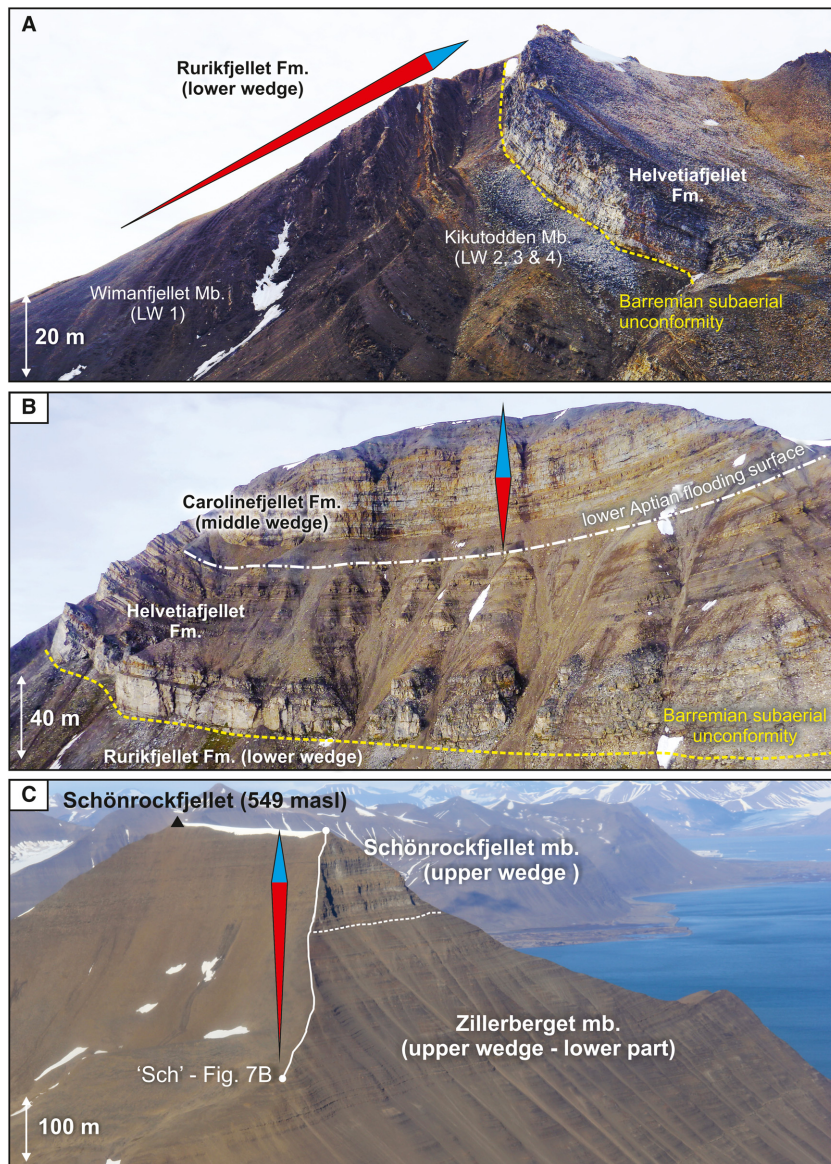
There has been a renewed interest in the Lower Cretaceous succession in Svalbard for the past few years due to increased exploration efforts on the Barents Shelf. Marin *et al.* (2016) documented a clinoform succession on the shelf south of Svalbard, whereas Grundvåg *et al.* (2017) presented regional onshore to offshore correlations. Olausen *et al.* (2018) summarizes the Mesozoic development of easternmost Svalbard, including parts of the Lower Cretaceous succession. By integrating outcrop and onshore subsurface data, Grundvåg *et al.* (2019) documented the depositional architectures of the lower and middle wedges and discussed their link to the paralic Helvetiafjellet Formation. Śliwińska *et al.* (2020) presented an updated biostratigraphic framework for the lower wedge and the overlying paralics. Jelby *et al.* (2020) investigated the facies variability and origin of storm deposits of the lower wedge in the northern part of the outcrop window, whereas the facies architecture of a coarse-grained lateral equivalent wedge in southern Spitsbergen was documented by Grundvåg & Olausen (2017). The present study summarizes some of the recent findings, and offers a detailed description of the little studied upper wedge, including a comprehensive comparison to the well-documented middle and lower wedges. This has never been done before.

### Storm-bed architecture and variability

A total of 19 bed types are recognized according to bed thickness, external geometry and internal facies architecture (BT 1 to BT 19; Fig. 9). Although bed thicknesses may vary significantly within a single bed, the beds are classified as *thick* (0.5 to 3.5 m), *medium* (0.2 to 1.0 m) or *thin* (0.2 to 0.01 m). The term 'bed type' refers here to a storm-deposited event bed, thus conforming to a *tempestite*. Most of the thin beds record deposition following the passage of a single storm event, whereas a large portion of the thicker beds shows signs of amalgamation, indicating multiple episodes of storm deposition and reworking. In addition, four principal types of mudstone-dominated 'background' deposits are recognized (Fig. 9).

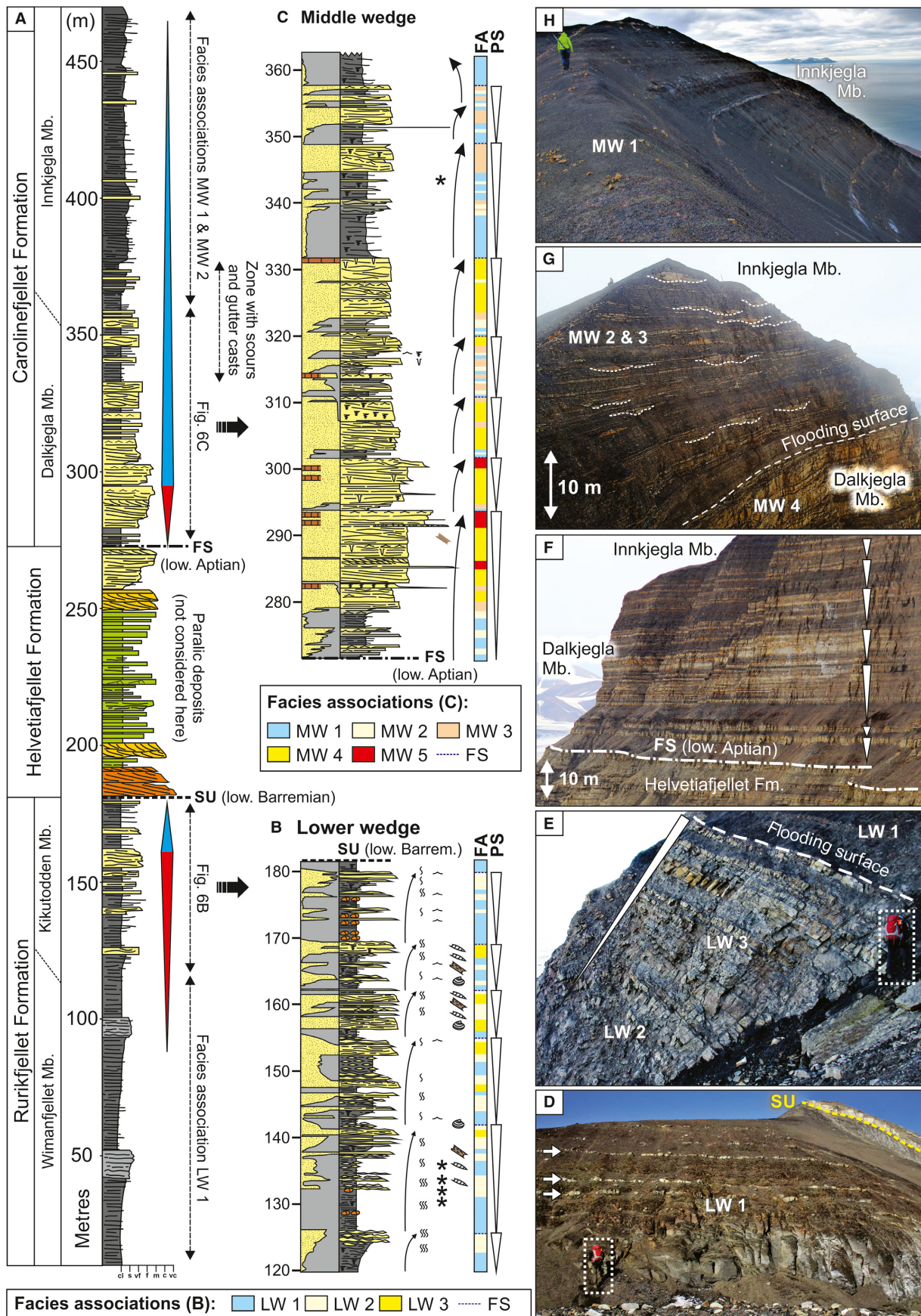
#### *Thin-bedded tempestites*

*Description.* This group of beds include BT 1 to BT 7, and consists of normally-graded siltstone



**Fig. 5.** Representative outcrop photographs of the Rurikfjellet and Carolinefjellet Formations from different parts of Spitsbergen. (A) Overview of the lower wedge showing the stratigraphic distribution of facies associations (LW 1 to LW4) at Ramfjellet in the northernmost part of the outcrop belt. (B) Overview of the middle wedge and the lower Aptian flooding surface separating the Carolinefjellet and Helvetiafjellet formations at Annaberget. (C) Overview of the west face and summit of Schönrockfjellet (549 metres above sea level, masl), showing the excellent exposures of the upper wedge (that is the Zillerberget and Schönrockfjellet members). The positions of the localities are given in Fig. 2B. Red and blue triangles indicate prograding and retrograding parasequence sets (*sensu* Van Wagoner *et al.*, 1990), respectively.

**Fig. 6.** Stratigraphic setting of the lower and middle wedges. (A) Sedimentary log from the Festningen outcrop section showing the parasequence arrangement of the lower (LW) and middle (MW) wedges, vertical distribution of facies associations (LW 1 to LW 3 and MW 1 to MW 5), and their stratigraphic relationship to the intercalated paralic deposits of the Helvetiafjellet Formation. (B) Detailed log of the lower wedge. Notice the heterolithic character of the wedge compared to the middle wedge shown in (C). (D) The shale-dominated lower part of the lower wedge (i.e. the Wimanfjellet Member) at Baronfjella. (E) Details of a sandstone-rich parasequence (marked by white triangle) in the upper part of the lower wedge (that is the Kikutodden Member) at Forkastningsfjellet. (F) Example of the parasequence arrangement of the middle wedge at Båtsmannen. Note how it becomes more heterolithic upward. (G) Scours and gutter casts (demarcated by dashed lines) commonly occur in the upper part of the middle wedge at the transition between the Dalkjegla and Innkjegla Members. Example from Louiseberget. (H) The sandstone-dominated part of the middle wedge grades upward into a several hundred metres thick shale-dominated succession (that is the Innkjegla Member), example from Baugen. FS: lower Aptian flooding surface, SU: lower Barremian subaerial unconformity. For locations, see Fig. 2B. (I) Legend for all the sedimentary logs, photographs and sketches shown in this paper. People for scale are *ca* 1.8 m tall.



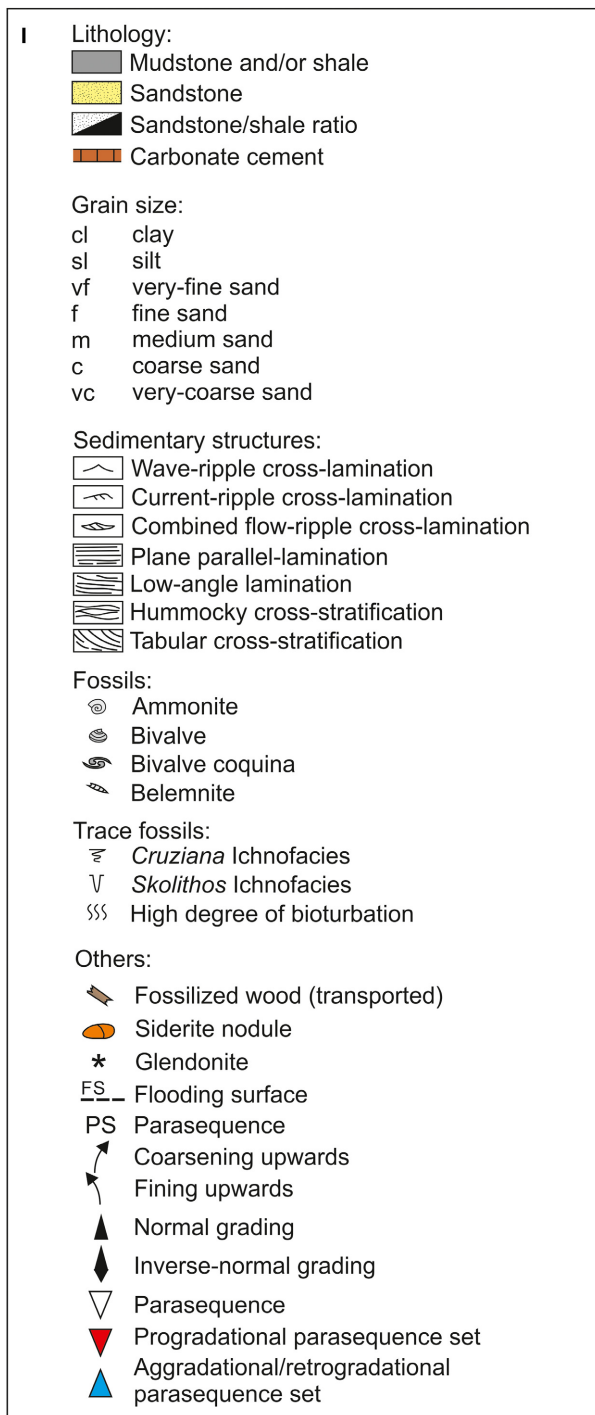


Fig. 6. Continued.

and very fine to fine-grained sandstone beds locally containing gravel conglomerates (Fig. 9). BT 1 consists of sharp-based siltstone beds characterized by abundant bioturbation (Fig. 10A). BT 2 is characterized by thin (<5 cm) lenticular

to wavy-bedded sandstone beds exhibiting wave-flow or, less frequently, combined-flow ripple cross-lamination, commonly forming tabular to wedge-shaped heterolithic units some few decimetres to several metres thick (Figs 11A and 12B). In some cases, these heterolithic deposits fill in several metres wide and <1 m deep scours (Fig. 13A; Jelby *et al.*, 2020). BT 3 consists of beds with tabular to pinch-and-swell geometries displaying isotropic HCS and wave-rippled to gradational and bioturbated bed tops (Fig. 10B and C). BT 3 is commonly interbedded with the heterolithics of BT 1 and BT 2 (Fig. 12B). Couplets consisting of sandstone and carbonaceous laminae (Fig. 10C), and small gutter casts (<20 cm thick and some few decimetres wide; Fig. 13F) occur in some beds. Jelby *et al.* (2020) have also documented double mud drapes in these beds. BT 4 consists of normally-graded beds with plane parallel lamination (PPL) to quasi-planar lamination (QPL; *sensu* Arnott, 1993) in their lower part, and current-flow to combined-flow ripple cross-lamination in their upper part (Fig. 10D). Climbing ripple sets are very common (Jelby *et al.*, 2020). BT 5 consists of sharp-based sandstone beds with a marked coarser-grained lower division (up to coarse sand) and a gradationally overlying upper division exhibiting PPL to QPL. BT 6 consists of sharp-based, lenticular beds typically characterized by a commonly inversely graded, gravel-rich lower division and a normally graded upper medium to fine-grained sandstone division exhibiting swaley cross-stratification (SCS; *sensu* Leckie & Walker, 1982), PPL or QPL (Fig. 10E; Jelby *et al.*, 2020). BT 7 is relatively rare, and consists of sharp-based beds containing a clast-supported lithic conglomerate lower division, sharply overlain by an upper division exhibiting climbing combined flow-ripple to current-ripple cross-lamination (Figs 9 and 11B).

*Interpretation.* Based on the normal grading, siltstones of BT 1 are interpreted as the deposits of storm-wave-suspended sediment clouds representing the distal wake of waning storms. Sharp and erosive bases suggest that some beds were deposited by low-density turbidity currents (Grundvåg *et al.*, 2014; Jelby *et al.*, 2020). The thin, lenticular-bedded and heterolithic nature of BT 2, indicates deposition under fluctuating energy conditions close to SWB. The sandstone lenses with wave-ripple cross-lamination record deposition by storm-waves with very low orbital

velocities and short wavelengths (Dott & Bourgeois, 1982). Combined flow-ripple cross-lamination indicates bedform migration under the combined action of oscillatory and unidirectional flows. The pinch-and-swell geometries, isotropic HCS and wave-rippled bed tops suggest that BT 3 records deposition by storm-waves with low orbital velocities and short wavelengths under waning storm activity (Dott & Bourgeois, 1982). Couplets of sandstone and carbonaceous laminae, as well as double mud drapes may indicate some tidal influence (Jelby *et al.*, 2020).

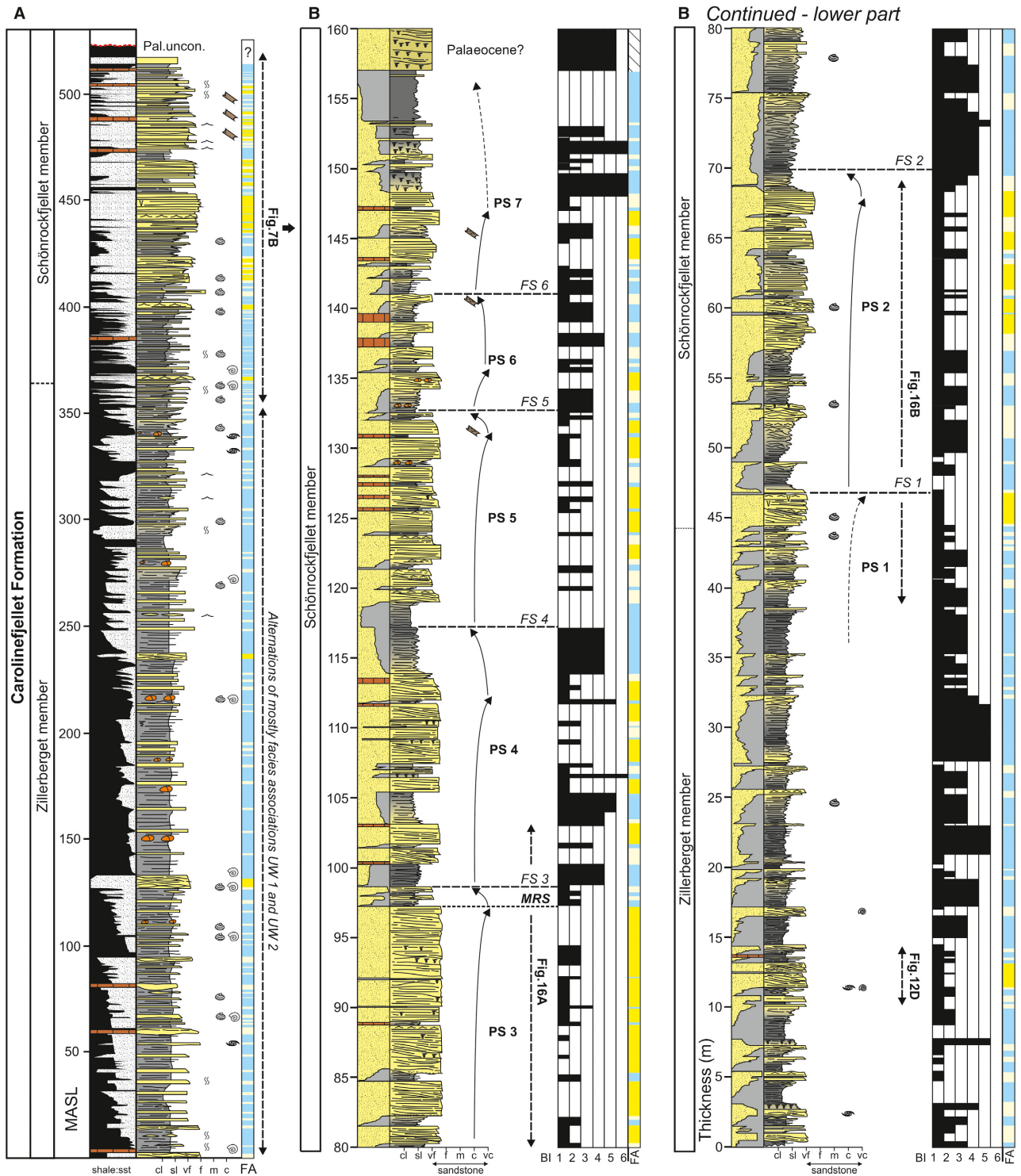
Beds BT 4 to BT 7 all exhibit sharp erosive bases, normal grading and successions of sedimentary structures indicating initial erosion followed by penecontemporaneous traction deposition and suspension fallout from waning wave-modified turbidity currents (*sensu* Myrow *et al.*, 2002; Jelby *et al.*, 2020). The presence of climbing ripple sets may indicate rapid deposition and high rates of aggradation either as a result of abrupt storm cessation or flow expansion due to loss of flow confinement (possibly down-dip of scours or low-sinuosity channels of BT 10). Inverse to normally graded, gravel-rich beds (BT 6) may reflect deposition by waxing-waning hyperpycnal flows (Mulder *et al.*, 2003; Bhattacharya & MacEachern, 2009).

#### *Medium-bedded tempestites*

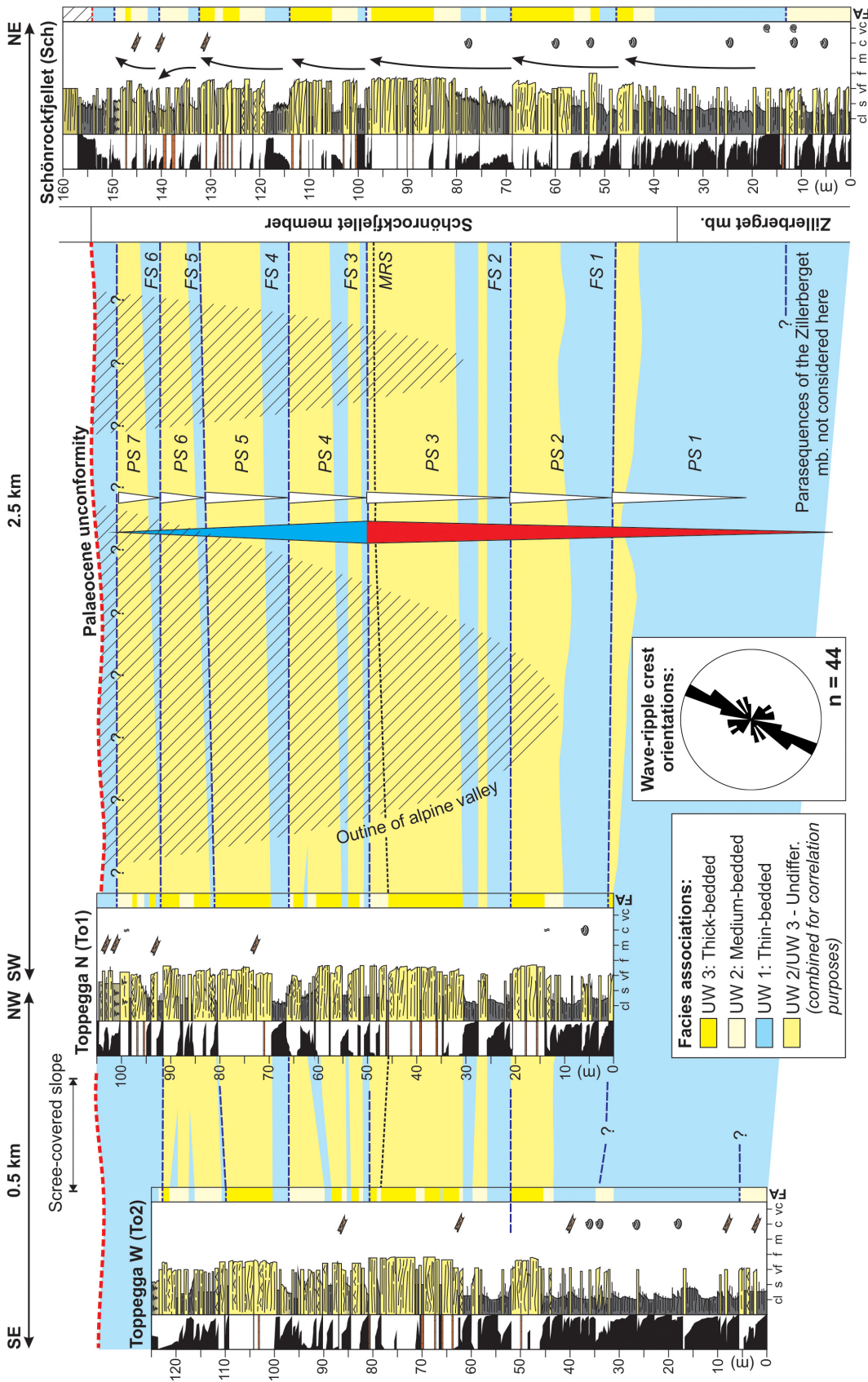
**Description.** This group of beds include BT 8 to BT 15, and consists of normally to weakly graded, very fine to fine-grained sandstone beds with tabular geometries and sharp bases, or lenticular beds with irregular to concave-up erosive bases (Fig. 9). BT 8 is characterized by commonly siderite-cemented, lenticular sandstone-beds with a lower shell-rich division consisting of horizontally oriented, concave-up disarticulated bivalves (Fig. 12E and F). The PPL, isotropic HCS and combined flow-ripple to wave-ripple cross-lamination occur in the upper bed division (Fig. 12F). BT 9 is characterized by isotropic HCS sandstone beds, which contain amalgamation surfaces and laterally splay into thinner sandstone beds (i.e. BT 3) exhibiting isotropic HCS and marked pinch-and-swell geometries (Fig. 9). These beds commonly transit laterally into BT 10, which consists of amalgamated, isotropic or low-angle anisotropic HCS sandstone beds confined to several metres wide and up to 1 m deep scours with steep-walled and 'stepped' margins (Fig. 13C and D). Occasionally, the scour infill has a more compound

architecture characterized by laterally accreted beds (Fig. 9). BT 11 consists of weakly graded, tabular to wedge-shaped sandstone beds containing shingled lamina sets separated by low-angle second-order truncation surfaces (Fig. 11C). Low-relief scoured bases are evidenced by the abrupt termination of the shingled lamina sets (Figs 9 and 11C). The PPL, QPL, rippled bed tops and gutter casts occur locally (Fig. 13E). BT 12 consists of anisotropic HCS sandstone beds with tabular or asymmetrical lenticular geometries (Fig. 11D and E). Basal scours are common (Fig. 10F). BT 13 consists of isotropic HCS sandstone beds with tabular to pinch-and-swell geometries, and wave-rippled bed tops (Figs 9, 10G and 12G). Some beds have scoured and undulating bases (Figs 10G and 13B). Complex facies arrangements (*sensu lato* Jelby *et al.*, 2020) occur locally as intra-bed horizons of wave-ripple to combined flow-ripple cross-lamination, or convolute lamination. BT 14 consists of normally-graded, medium to fine-grained sandstone beds exhibiting PPL or QPL (Figs 10H and 13A). Gutter casts and combined flow-rippled tops are sporadically present (Fig. 11F). BT 15 consists of normally or inverse to normally graded medium to fine-grained sandstone beds typically confined to several metres long and up to 0.8 m deep scours with 'stepped' margins (Fig. 10G and I). Basal gravel lags and internally scattered gravel lenses occur frequently (Jelby *et al.*, 2020). Swaley cross-stratification (*sensu* Leckie & Walker, 1982), isotropic HCS and QPL are variably present (Fig. 10I).

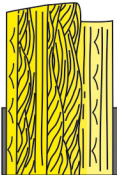
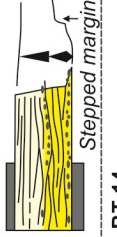
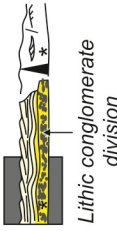
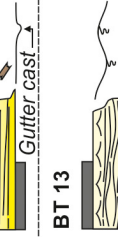
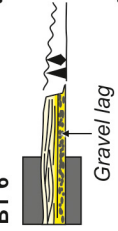
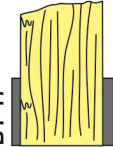
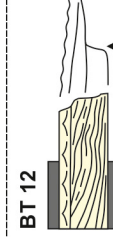
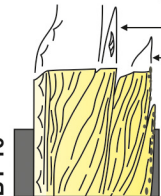
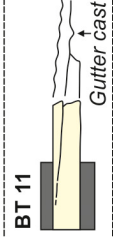
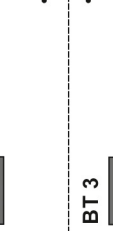
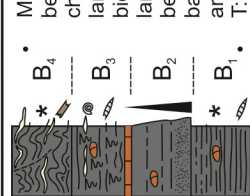
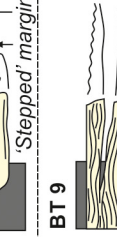
**Interpretation.** The erosional scours of BT 8 are interpreted to have been cut by strong unidirectional flows generated during the waxing and peak stage of storms (e.g. Myrow, 1992a; Collins *et al.*, 2017; Olaussen *et al.*, 2018). The associated scour infill was deposited during waning storm conditions under the influence of combined and oscillatory-dominated combined flow. Shell debris indicates strong winnowing and the presence of shell banks that provided local carbonate sources. The isotropic HCS and wave-rippled bed tops of BT 9 indicate deposition by oscillatory storm-waves under waning storm activity. The amalgamated character and splaying of beds point to reworking by multiple storm events. The erosional scours of BT 10 are similar to those of BT 8, but commonly exhibit stepped margins and compound fills, which indicate reoccupation and multiple episodes of erosion



**Fig. 7.** Representative logs of the upper wedge. (A) Composite sedimentary log of the upper wedge (that is the Zillerberget and Schönrockfjellet members) from the Schönrockfjellet outcrop section. The lower 400 m of the succession is dominated by thin-bedded heterolithics consisting of facies associations (FA) UW 1 and UW 2, whereas the upper part is dominated by thick-bedded storm deposits of FA UW 3. Based on Århus (1991), Grundvåg *et al.* (2015) and Hurum *et al.* (2016). (B) Detailed sedimentological log through the upper part of the upper wedge, including sedimentary structures and lithologies, facies association distribution, parasequences (PS 1 to PS 7), and bioturbation intensity (BI; *sensu* Taylor & Goldring, 1993). For location of the section, see Figs 2C and 5C. MRS: maximum regressive surface. Legend is given in Fig. 6I. MASL = metres above sea level.



**Fig. 8.** Correlation panel of the three measured sections through the upper wedge at Schönrockfjellet (Sch) and Toppegga (To1 and To2) showing the lateral and vertical distribution of facies associations UW 1 to UW 3. Fig. 2C for location. Notice the tabular architecture of the investigated parasequences (PS 1 to PS 7, marked by white triangles) bounded by flooding surfaces (FS 1 to FS 6) and the Palaeocene unconformity. PS 1 to PS 3 show progradational stacking (marked by red inverse triangle), and PS 4 to PS 7 show aggradational stacking (blue triangle). A maximum regressive surface (MRS) separates the two parasequence sets. Measured wave ripple crests display a NNE–SSW orientation, possibly indicating a roughly north to south-oriented palaeoshoreline. The wave ripple population showing a north–west to south–east orientation is related to interference ripples with crests oriented perpendicular to the dominant north–east to south–west orientation. Legend is given in Fig. 6I.

<p><b>Thick-bedded tempestites</b></p> <p><i>Bed architecture:</i> <i>Description:</i></p>	<p><b>Medium-bedded tempestites</b></p> <p><i>Bed architecture:</i> <i>Description:</i></p>	<p><b>Thin-bedded tempestites</b></p> <p><i>Bed architecture:</i> <i>Description:</i></p>
<p><b>BT 19</b></p>  <ul style="list-style-type: none"> <li>Amalgamated, medium to coarse-grained sandstone beds forming tabular units characterized by rough cross-bedding and PPS. Wave-ripple cross-lamination occurs locally.</li> <li>T: 0.5-2 m</li> </ul>	<p><b>BT 15</b></p>  <p><i>Stepped margin</i></p> <ul style="list-style-type: none"> <li>Erosively based sandstone beds exhibiting SCS and PPL to QPL. Basal and internal gravel lags occur frequently.</li> <li>T: 0.4-0.6 m</li> </ul>	<p><b>BT 7</b></p>  <p><i>Lithic conglomerate division</i></p> <ul style="list-style-type: none"> <li>Normally graded sandstone beds with a lower lithic conglomerate division. Wavy lamination, climbing combined flow- and current-ripple cross-lamination in the upper part.</li> <li>T: 0.1-0.3 m</li> </ul>
<p><b>BT 18</b></p>  <ul style="list-style-type: none"> <li>Tabular and amalgamated bed successions with horizontal to undulating erosive bases and aligned rip-up mudstone clasts. Isotropic HCS and PPS dominate. Wave-rippled bed tops and internal truncations occur.</li> <li>T: 1-3.5 m</li> </ul>	<p><b>BT 14</b></p>  <p><i>Gutter cast</i></p> <ul style="list-style-type: none"> <li>Tabular sandstone beds exhibiting PPL to QPL. Wave-rippled bed tops are present.</li> <li>T: 0.4-0.8 m</li> </ul>	<p><b>BT 6</b></p>  <p><i>Gravel lag</i></p> <ul style="list-style-type: none"> <li>Sandstone beds with a coarse-grained, gravel-rich lower division, and SCS, PPL to QPL in the upper part. Generally undulating bed tops.</li> <li>T: 0.1-0.2 m</li> </ul>
<p><b>BT 17</b></p>  <ul style="list-style-type: none"> <li>Sandstone beds with tabular or pinch-and-swell geometries displaying PPS in the lower part, isotropic HCS in the upper part, and sharp bed-tops.</li> <li>T: 0.9-2 m</li> </ul>	<p><b>BT 13</b></p>  <p><i>Accretionary to scour-and-drape HCS</i></p> <ul style="list-style-type: none"> <li>Isotropic HCS sandstone beds with tabular or pinch-and-swell geometries. 'Complex' facies sequences occur locally. Wave-rippled bed tops occur frequently.</li> <li>T: 0.3-0.8 m</li> </ul>	<p><b>BT 5</b></p>  <ul style="list-style-type: none"> <li>Sharp-based, normally-graded, tabular-shaped sandstone beds with PPL to QPL.</li> <li>T: 0.1-0.2 m</li> </ul>
<p><b>BT 16</b></p>  <p><i>Tapering beds</i></p> <ul style="list-style-type: none"> <li>Several tens of metres long, 'compound' sandstone bodies consisting of accreted, sigmoidal beds separated by internal truncation surfaces. PPS, QPL, isotropic to anisotropic HCS and wave-rippled bed tops occur.</li> <li>T: 0.5-1.5 m</li> </ul>	<p><b>BT 12</b></p>  <p><i>Scour margin</i></p> <ul style="list-style-type: none"> <li>Tabular to wedge-shaped, sharp-based sandstone beds with anisotropic HCS. Scoured bases and wave-rippled bed tops are common.</li> <li>T: 0.2-0.4 m</li> </ul>	<p><b>BT 4</b></p>  <ul style="list-style-type: none"> <li>Sandstone beds with PPL to QPL in the lower part and combined flow- to current-ripple cross-lamination in the upper part (commonly climbing sets).</li> <li>T: 0.1-0.3 m</li> </ul>
<p><b>'Background' mudstone deposits</b></p>  <ul style="list-style-type: none"> <li>Mudstone-dominated interbeds and bed successions of varying facies characteristics including: 1) finely laminated, 2) graded to non-graded, 3) bioturbated, and 4) convoluted laminated mudstone beds. Ammonites, belemnites, glendonites, siderite bands (with cone-in-cone structures) and concretions occur sporadically.</li> <li>T: 0.01-200 m</li> </ul>	<p><b>BT 11</b></p>  <p><i>Gutter cast</i></p> <ul style="list-style-type: none"> <li>Tabular, graded to PPL and QPL sandstone beds with shingled lamina sets.</li> <li>T: 0.2-0.5 m</li> </ul>	<p><b>BT 3</b></p>  <p><i>Gutter cast</i> <i>Carbonaceous laminae</i></p> <ul style="list-style-type: none"> <li>Tabular to lenticular (dm- to m-scale) sandstone beds with isotropic HCS (accretionary to scour-and-drape type). Wave-rippled bed tops occur frequently. Rare gutter casts.</li> <li>T: 0.05-0.3 m</li> </ul>
<p>Legend:</p> <ul style="list-style-type: none"> <li>Sandstone (M/C-grained)</li> <li>Sandstone (Vf-F-grained)</li> <li>Sandstone (F-grained)</li> <li>Mudstone (undiffer.)</li> </ul>	<p><b>BT 9</b></p>  <ul style="list-style-type: none"> <li>Amalgamated, isotropic HCS sandstone beds splitting into thinner beds laterally. Wave-rippled bed tops are present.</li> <li>T: 0.3-0.7 m</li> </ul>	<p><b>BT 2</b></p>  <p><i>Scour base</i></p> <ul style="list-style-type: none"> <li>Thin, lenticular (cm-scale) sandstone beds with combined flow to wave-ripple cross-lamination. Form tabular to wedge-shaped heterolithic units (a few dm to &gt;10 m thick).</li> <li>T: 0.01-0.05 m</li> </ul>
	<p><b>BT 8</b></p>  <p><i>Siderite cement</i> <i>Aligned shells</i></p> <ul style="list-style-type: none"> <li>Erosively based, lenticular sandstone beds displaying PPL to HCS and wave-rippled bed tops. Disarticulated bivalves form basal lags.</li> <li>T: 0.2-0.5 m</li> </ul>	<p><b>BT 1</b></p>  <ul style="list-style-type: none"> <li>Sharp-based, graded to non-graded siltstone beds. Sandy bioturbation.</li> <li>T: 0.1-0.3 m</li> </ul>

**Fig. 9.** Schematic illustration of the 19 tempestite bed types and various ‘background’ mudstone deposits recognized in the three wedge (BT 1 to BT 19), partly based on Jelby *et al.* (2020). The tempestite beds are classified as thick-bedded (T: 0.5–3.5 m), medium-bedded (T: 0.2–1.0 m) or thin-bedded (T: 0.01–0.2 m thick). See text for detailed description and process interpretation. HCS: hummocky cross-stratification, PPL: plane parallel lamination, PPS: plane parallel stratification, QPL: quasi-planar lamination, SCS: swaley cross-stratification.

and deposition within the same scour (e.g. Collins *et al.*, 2017). The presence of anisotropic HCS suggests that some scours were filled by deposits from current-dominated combined flows, whereas laterally accreted beds indicate that some flows were of possibly helicoidal character (Nøttvedt & Kreisa, 1987; Myrow, 1992b; Midtgaard, 1996; Tinterri, 2011; Eide *et al.*, 2015). Some of the scours may thus represent low-sinuosity, shore-normal storm-surge channels (e.g. Amos *et al.*, 2003; Jelby *et al.*, 2020). BT 11 and BT 12 were deposited by similar formative processes, involving a phase of scouring followed by deposition from combined flows with a unidirectional component strong enough to form and initiate migration of dune-like bedforms (Myrow, 1992b). The accretionary isotropic HCS of BT 13 indicates deposition by sustained high-intensity oscillatory flows or oscillatory-dominated combined flows with high aggradation rates (Arnott & Southard, 1990; Duke *et al.*, 1991). The occurrence of scour-and-drape isotropic HCS indicates fluctuations in oscillatory-flow intensity causing local scour of the sediment surface (Cheel & Leckie, 1993). Flow-intensity variations and unsteady flows also explain the local occurrence of internal wave-rippled and/or convolute laminated horizons (i.e. the complex HCS configuration of Jelby *et al.*, 2020). The wave-rippled tops record reworking by low-intensity oscillatory flow during waning storm activity (Dott & Bourgeois, 1982). The erosive base, normal grading, PPL to QPL, and occasionally combined flow-rippled bed tops of BT 14, indicate erosion succeeded by traction deposition in upper-flow regime conditions by waning oscillatory-dominated combined flows (Arnott & Southard, 1990; Arnott, 1993). The scoured base, inverse to normal grading (i.e. wax-wane configuration), scattered gravel lags and lenses, and the abundant SCS (in medium-grained sandstone) indicate that BT 15 was deposited by sustained hyperpycnal flows modified by strong, steady storm-waves (Jelby *et al.*, 2020). Fluctuations in flow intensity and flow competence, and storm-wave orbital velocity resulted in localized cut-and-fill

structures demarcated by basal gravel lags and SCS. Similar, albeit larger, channel-like elements filled by hyperpycnal flow deposits have been described from prodelta to delta front and fluviually-influenced shoreface successions elsewhere (e.g. Pattison *et al.*, 2007; Ponce *et al.*, 2008; Tinterri, 2011; Eide *et al.*, 2015).

#### *Thick-bedded tempestites*

**Description.** This group of beds includes BT 16 to BT 19, and consists of weakly to non-graded, fine to medium-grained, amalgamated sandstone beds (Fig. 9). BT 16 consists of several tens of metres long (generally <30 m) and up to 1.5 m thick, ‘compound’ sandstone bodies (for example, Fig. 1C) characterized by progradationally (or laterally) accreted and locally compensationally stacked, sigmoidal beds separated by regular-spaced, low-angle dipping truncation surfaces (Figs 9 and 11G). Reactivation surfaces, PPS, QPL and isotropic to anisotropic HCS are variably present. Wave-rippled bed tops are common. BT 17 is characterized by tabular to low-relief pinch-and-swell-type beds with plane parallel stratification (PPS) in their lower part and isotropic HCS in their upper part. BT 18 consists of up to 3.5 m thick, highly amalgamated, tabular bed successions containing frequent internal truncation surfaces with aligned rip-up mudstone clasts (Fig. 11H). BT 19 consists of alternations of fine to medium-grained sandstone exhibiting PPS and wave-ripple cross-laminations, and erosively-based, medium to coarse-grained sandstone displaying trough cross-stratification (Fig. 11I).

**Interpretation.** Based on the compound architecture and laterally accreted, sigmoidal beds exhibiting various oscillatory-flow and combined flow-generated sedimentary structures, BT 16 is interpreted as large-scale, migrating bedforms deposited by recurrent storm-generated combined flows (Nøttvedt & Kreisa, 1987; Midtgaard, 1996). Although the sandstone bodies clearly record the amalgamation of multiple storm events, they show many similarities to tidal-generated compound bedforms described elsewhere (for example, regular and laterally

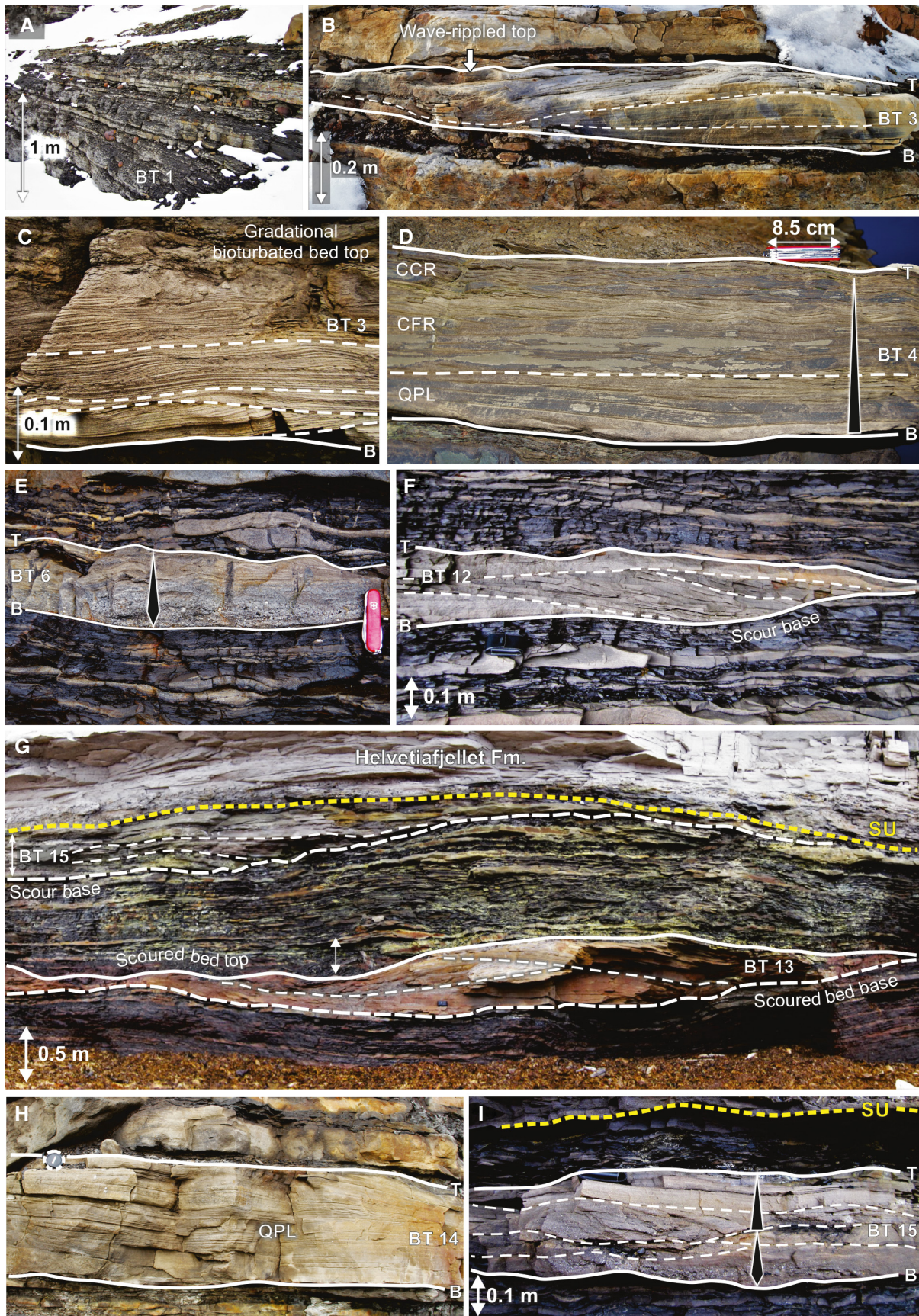


**Fig. 10.** Representative photographs of various storm beds observed in the lower wedge (note that the shown bed types are not necessarily unique to the lower wedge). (A) Sharp-based siltstone beds of BT 1. (B) An isolated, non-amalgamated bed displaying isotropic HCS and a wave-rippled top (BT 3). Dashed lines indicate internal second-order truncation surfaces. (C) An example of carbonaceous laminae within a BT 3 bed with a gradational and bioturbated top. Stippled lines indicate internal second-order truncation surfaces. This variety of BT 3 only occurs in the lower wedge (i.e. the Kikutodden Member). (D) An example of a BT 4 bed displaying normal grading (marked by triangle), quasi planar lamination (QPL), combined flow-ripple cross-lamination (CFR), and climbing current ripple cross-lamination (CCR) (see Jelby *et al.*, 2020 for a detailed delineation of this bed). (E) Wax-wane configuration (marked by the white pseudo-triangle) of a sharp-based, gravel-rich, quasi-planar-laminated sandstone bed (BT 6) with abundant coal clasts, organic debris and a combined-flow rippled bed top (Jelby *et al.*, 2020). Pocket knife (8.5 cm) for scale. (F) An anisotropic HCS sandstone bed with a scoured base and wave-rippled bed top (BT 12). Stippled lines indicate shingled lamina sets with preferred dip orientations. In the lower wedge, this bed type only occurs in facies association LW 4 confined to the uppermost parasequence of the unit. (G) In the uppermost parasequence of the lower wedge, multiple scour surfaces defines the base of BT 13 and BT 15 beds (see Jelby *et al.*, 2020 for a detailed delineation of the upper scour infill), or the base of heterolithic scour-and-fill units cutting into underlying storm beds (marked by double arrow). (H) and (I) show examples of (commonly gravel-rich) sharp-based, erosional beds displaying QPL (BT 14) to swaley cross-stratification (SCS; BT 15). These beds were deposited by powerful, unidirectional (wave-modified) flows, possibly of hyperpycnal origin. B: bed base, T: bed top. Lens cap (5 cm) for scale in (H).

spaced truncation surfaces, reactivation surfaces and sigmoidal foreset geometries; Olariu *et al.*, 2012; Leva López *et al.*, 2016), possibly reflecting storm-wave and tidal current interactions. Isotropic HCS and PPS in BT 17 and BT 18 indicate deposition by high-intensity oscillatory-dominated flow, whereas the amalgamated character of BT 18 points to deposition and reworking by multiple storm events, near or possibly slightly above fair-weather wave base (FWWB). Thick-bedded and amalgamated tempestite beds are commonly attributed to deposition in proximal and shallower settings influenced by frequent storms and large waves (e.g. Dott & Bourgeois, 1982; Brenchley *et al.*, 1986, 1993). The coarse-grained character, and alternations of trough cross-stratification and PPS, suggest traction in upper flow regime conditions for BT 19. The trough cross-stratification represents migrating three-dimensional dunes formed by unidirectional flow, possibly induced by breaking waves above FWWB (e.g. Dumas & Arnott, 2006). The PPS records periods of increased flow velocities, probably reflecting sheet-flow conditions induced by very asymmetrical, high-intensity oscillatory flow (e.g. Clifton, 1976; Dumas & Arnott, 2006). The interbedded horizons of wave ripple cross-lamination record episodes of oscillatory flow of lowered intensity.

#### 'Background' mudstone deposits

**Description.** This group of mudstone-dominated facies include: B<sub>1</sub> (laminated), B<sub>2</sub> (graded to non-graded and homogenous, commonly sharp-based), B<sub>3</sub> (bioturbated) to B<sub>4</sub> (convolute

laminated and syn-sedimentary faulted; Fig. 9), and occurs as: (i) thin (<0.1 m) interbeds in heterolithic to sandstone-dominated successions; (ii) thin (<0.5 m) beds separating and encapsulating isolated storm-deposited sandstone beds; or (iii) metres to several tens of metres thick (<200 m), laterally extensive mudstone-dominated successions (for example, Fig. 5A). Streaks of siltstone and sandstone are variably present in all of the mudstone bed types, but occur more frequently in B<sub>4</sub>. Siderite bands (occasionally with 'cone in cone' structures) and concretions (commonly strata-bound), glendonites, belemnites, ammonites, bivalves and fossil wood occur sporadically throughout the mudstone-dominated facies.

**Interpretation.** A wide range of processes may be responsible for the deposition of mud on storm-dominated shelves (Bhattacharya & MacEachern, 2009; Macquaker *et al.*, 2010; Plint, 2014; Wilson & Schieber, 2015). The laminated character of B<sub>1</sub> indicates deposition by hemipelagic fallout below SWB. The commonly sharp-based, graded to non-graded, and homogenous character of B<sub>2</sub> suggests deposition by rapid suspension fallout of fluid mud from wave-generated flocculations, rapid mud aggradation under collapsing hypopycnal sediment plumes, or highly concentrated, low-density turbidity currents, possibly of hyperpycnal origin (Parsons *et al.*, 2001; Lamb *et al.*, 2008; Varban & Plint, 2008; Bhattacharya & MacEachern, 2009; Jelby *et al.*, 2020). The abundant bioturbation of B<sub>3</sub> hampers any proper process interpretation of the mud itself. However, the high intensity of bioturbation indicates low rates of deposition

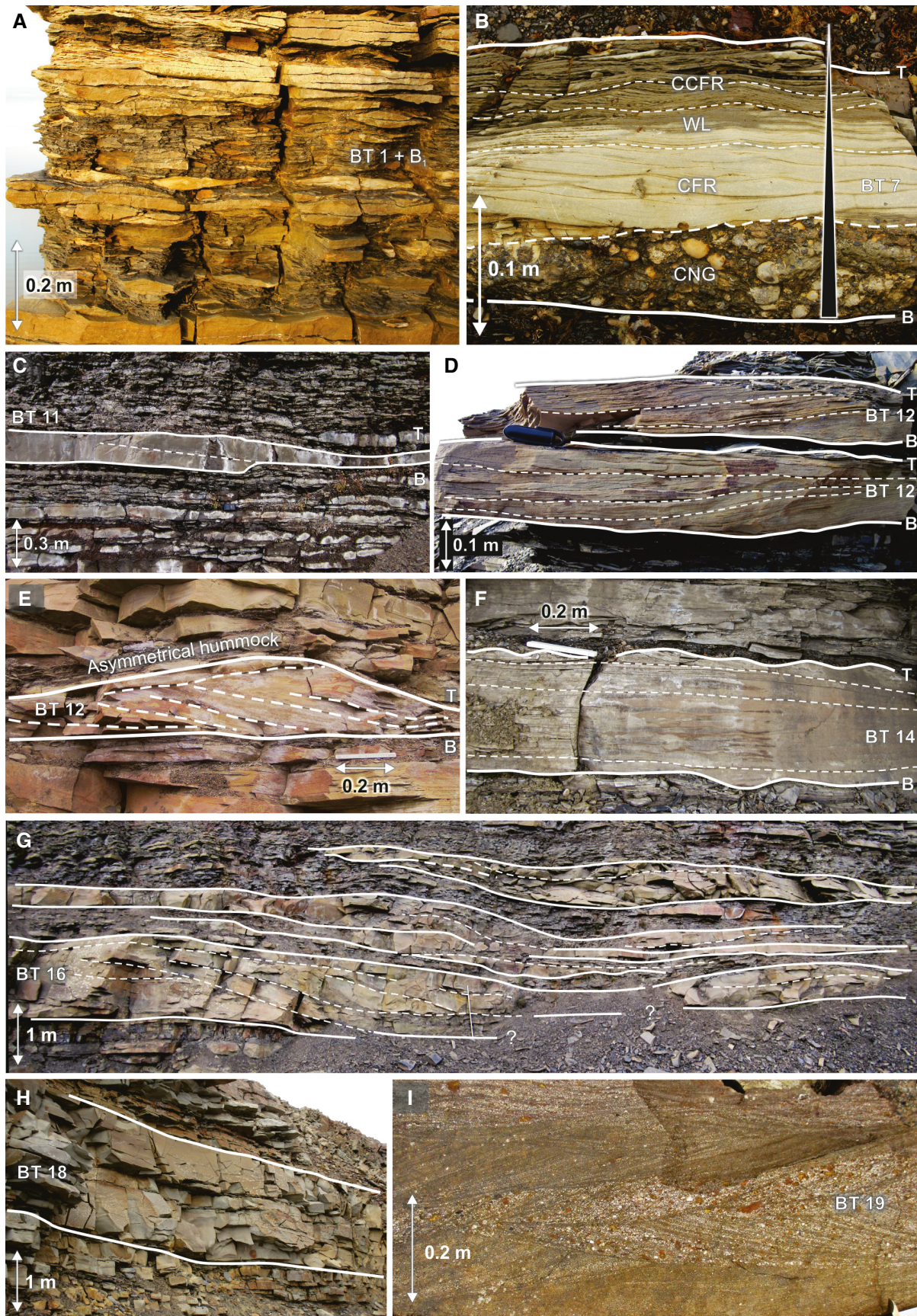


**Fig. 11.** Representative photographs of various storm beds observed in the middle wedge (note that the shown bed types are not necessarily unique to the middle wedge). (A) Interbedded background mudstone deposits and thin-bedded, lenticular storm beds of BT 2. (B) Rare example of a normally-graded, sharp-based BT 7 bed displaying a conglomeratic (CNG) lower division and an upper division exhibiting combined flow ripple cross-lamination (CFR), wavy lamination (WL) and climbing sets of combined flow ripple cross-lamination (CCFR). These beds are interpreted to represent deposits of wave-modified turbidity currents. (C) BT 11 is characterized by laterally accreted, and commonly abruptly terminating, lamina sets. (D) Two stacked beds with tabular geometries exhibiting laterally persistent low-angle anisotropic HCS (the most common variety of BT 12). (E) Rare example of a preserved asymmetrical hummocky bedform exhibiting anisotropic HCS. (F) A sharp-based, erosional sandstone bed displaying a gutter cast, plane parallel to quasi planar lamination and a combined flow rippled top (variety of BT 14; see Fig. 9 for details). (G) Example of a large-scale (several tens of metres long and up to 1.5 m thick) ‘compound’ hummocky sandstone body (e.g. Midtgaard, 1996; cf. Jelby *et al.*, 2020) consisting of laterally (or frontally) accreted and partly compensationally stacked sigmoidal beds separated by concordant discontinuity surfaces (BT 16). The accreted and compound architecture may point to deposition under the influence of tidal currents. (H) A thick-bedded, amalgamated sandstone unit characterized by isotropic HCS (BT 18). (I) Coarse-grained sandstone beds with trough cross-stratification only occur in the lowermost parasequences of the middle wedge in the north-western part of the outcrop window (at the Festningen and Ramfjellet localities, see Fig. 2B for location). B: bed base, T: bed top.

under quiescent, fully marine and oxygenated conditions (Wilson & Schieber, 2015). Traditionally, bioturbated mudstone beds within storm-deposited sandstone successions have been interpreted to represent fair-weather conditions (Dott & Bourgeois, 1982). The convolute-laminated and micro-faulted character of  $B_4$  indicates rapid deposition and subsequent post-depositional, gravitational-related deformation (Grundvåg *et al.*, 2014). The abundance of siltstone and sandstone streaks indicates the frequent passage and deposition by low-density turbidity currents or wave-enhanced hyperpycnal flows (Lamb *et al.*, 2008; Grundvåg *et al.*, 2014; Jelby *et al.*, 2020). Siderite bands and strata-bound concretions indicate periods of sediment starvation.

### Facies associations

Based on bed type distribution and abundance, as well as the relative proportion, of storm beds and ‘background’ mudstone deposits, a series of recurrent facies associations are recognized. The facies associations (FAs) are subdivided into those belonging to the lower (FAs LW 1 to LW 4), middle (FAs MW 1 to MW 5) and upper (FAs UW 1 to UW 3) wedges, despite some sedimentological similarities (summarized in Fig. 14).

#### *Facies associations of the lower wedge*

**Description.** Facies association LW 1 (‘mudstone-dominated deposits’; Fig. 14), consists mostly of  $B_1$  to  $B_3$  mudstone facies (Figs. 5A, 6A, 6D and 14), and is volumetrically the most important association of the lower wedge with a thickness exceeding 200 m across most of the study

area (Fig. 3C). The abundance of siltstone beds increases as LW 1 grades upward into LW 2.

Facies association LW 2 (‘thin to medium-bedded storm deposits’; Fig. 14) occurs as heterolithic units that consist of thin, lenticular to wavy-bedded, fine to very fine-grained sandstone beds (BT 2 and BT 3; Figs 6B and 14) alternating with thin mudstone and siltstone beds ( $B_2$  and BT 1; Fig. 10A). The sandstone beds exhibit wave-flow or combined-flow ripple cross-lamination (BT 2), as well as isotropic HCS in the thicker beds (BT 3). LW 2 commonly alternates with LW 3.

Facies association LW 3 (‘medium-bedded storm deposits’; Fig. 14) consists of medium-bedded, amalgamated to non-amalgamated, fine to very fine-grained, predominantly isotropic HCS sandstone beds (BT 3, BT 9 and BT 13; Fig. 10B). Individual beds are commonly sharp based and have wave-rippled tops. Trace fossils are variably present, mostly occurring in the upper part of the beds. Inverse to normally and normally-graded beds with PPL, QPL or SCS and climbing sets of combined-flow ripples (BT 4, BT 5 and BT 14; Fig. 10D), and anisotropic HCS sandstone beds occur locally (BT 12) (Jelby *et al.*, 2020).

Facies association LW 4 (‘heterolithic sandstone deposits with scours’; Fig. 14) only occurs in the uppermost part of the lower wedge in the northernmost study area (Fig. 15A). LW 4 comprises a *ca* 6 m thick heterolithic unit consisting of mudstones ( $B_2$  and  $B_4$ ) and siltstones (BT 1) passing upward into very fine to fine-grained sandstone beds exhibiting isotropic and anisotropic HCS, QPL to PPL, combined flow-ripple to wave-ripple cross-laminations, commonly occurring as climbing sets (BTs 3 to 6 and BTs

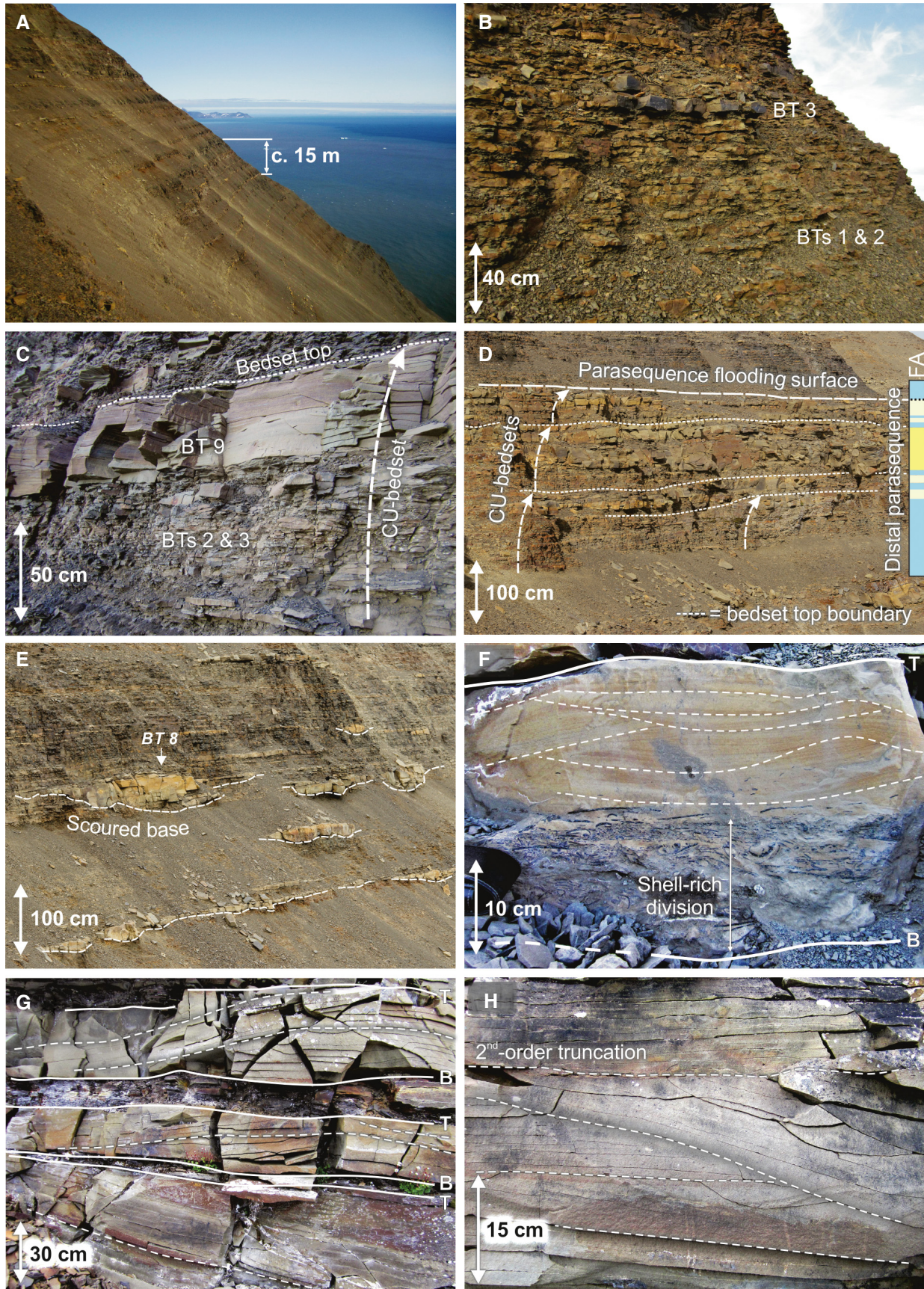


**Fig. 12.** Some typical features of the investigated tempestite beds of the upper wedge (that is the Zillerberget and Schönrockfjellet members). (A) Overview of facies association UW 1, which dominates the lower part of the upper wedge (that is the Zillerberget member). (B) Close-up view of facies association UW 1 in the Zillerberget member containing abundant thin-bedded, lenticular sandstone. These deposits are commonly characterized by sandstone to shale ratios of 30:70 to 70:30 (generally >50% sandstone). (C) Metre-scale, heterolithic coarsening-upward units (indicated by stippled arrow) are typical features in the Zillerberget member, and represent intra-parasequence bed-sets. (D) Locally, the bed-sets (indicated by stippled arrows) may stack vertically to form thicker heterolithic parasequences (marked by white triangle). (E) Commonly shell-rich and siderite-cemented storm beds with scoured bases occur sporadically within the thin-bedded heterolithics of the Zillerberget member (BT 8; Fig. 9 for details). (F) A shell-rich lower division characterizes BT 8. (G) The upper part of the upper wedge (that is the Schönrockfjellet member), is characterized by storm beds exhibiting isotropic HCS (BT 13). (H) Details of a bed displaying isotropic HCS. Note the second-order truncation surfaces (stipple lines) separating variably dipping lamina sets. The lamina set dip angles within these beds typically change rather abruptly across short distances (in contrast to the laterally persistent dip angles recorded in BT 12, Fig. 11D). B: bed base, T: bed top. All photographs are from Schönrockfjellet.

12 to 14; Figs 9, 10D, 10E and 10F; Jelby *et al.*, 2020). Lenses and basal lags of coarse-grained sandstone and gravel conglomerates occur in some beds (for example, BT 6 and BT 15; Fig. 10E and I; Jelby *et al.*, 2020). Medium-grained sandstone beds displaying SCS (BT 15, Fig. 10I), and scour-and-fill structures up to 1 m deep and several metres wide occur in places (Figs 10G, 13A and 13B; Jelby *et al.*, 2020). In well DH1 in Adventdalen (Fig. 15A), LW 4 is characterized by a *ca* 50 m thick sandy mudstone succession (dominated by B<sub>4</sub> deposits) passing upward into current ripple cross-laminated and soft-sediment deformed sandstones (only the upper 17 m shown in Fig. 15A). Plant material is abundant.

*Interpretation.* Based on the dominance of shale, facies association LW 1 is primarily attributed to deposition from suspension settling in a low-energy, offshore environment, generally below storm-wave base. Low-density turbidity currents, and highly concentrated storm-wave suspended fluid muds are the most reliable processes for the offshore mud accumulation (Wilson & Schieber, 2015; Grundvåg *et al.*, 2019; Jelby *et al.*, 2020). The upward increase in siltstone beds indicates shallowing and overall regressive conditions (Dypvik *et al.*, 1991a; Grundvåg *et al.*, 2017).

Based on the heterolithic character and predominance of sedimentary structures generated by oscillatory and oscillatory-dominated combined flows, facies association LW 2 is attributed to deposition between fair-weather and storm-wave base in a storm-dominated, offshore transition zone to lowermost shoreface setting

(Dott & Bourgeois, 1982; Dumas & Arnott, 2006; Grundvåg *et al.*, 2019). A storm-dominated lower shoreface setting is inferred from the abundance of thicker, isotropic HCS sandstone beds in the overlying, and commonly alternating, facies association LW 3. Normally-graded beds displaying anisotropic HCS, QPL and climbing ripples indicate deposition by waning wave-modified turbidity currents (Jelby *et al.*, 2020). Inverse to normally graded, gravel-rich beds (BT 6) record deposition from rare waxing-waning hyperpycnal flows (Jelby *et al.*, 2020).

The presence of a wide range of tempestite beds, commonly with features indicating deposition by unidirectional-dominated combined flow, frequent scour-and-fill features and abundant plant material, suggest a storm-dominated prodelta to distal delta front environment for facies association LW 4 (Nemec *et al.*, 1988; Jelby *et al.*, 2020). The scour-and-fill features may have been cut and filled by hyperpycnal flows derived from fluvial distributary channels further up-dip (Eide *et al.*, 2015; Jelby *et al.*, 2020), or they record erosion and subsequent infill by storm-generated offshore-directed oscillatory-dominated combined flows (Collins *et al.*, 2017).

#### *Facies associations of the middle wedge*

*Description.* Facies association MW 1 ('mudstone-dominated deposits'; Fig. 14) forms regionally extensive mudstone-dominated units in the lowermost and uppermost parts of the middle wedge (Fig. 6A, F and H). The lowermost shale unit is 10 to 30 m thick (Fig. 15B), dark-coloured, finely laminated and sparsely bioturbated. It rests unconformably on the underlying paralic deposits of the Helvetiafjellet

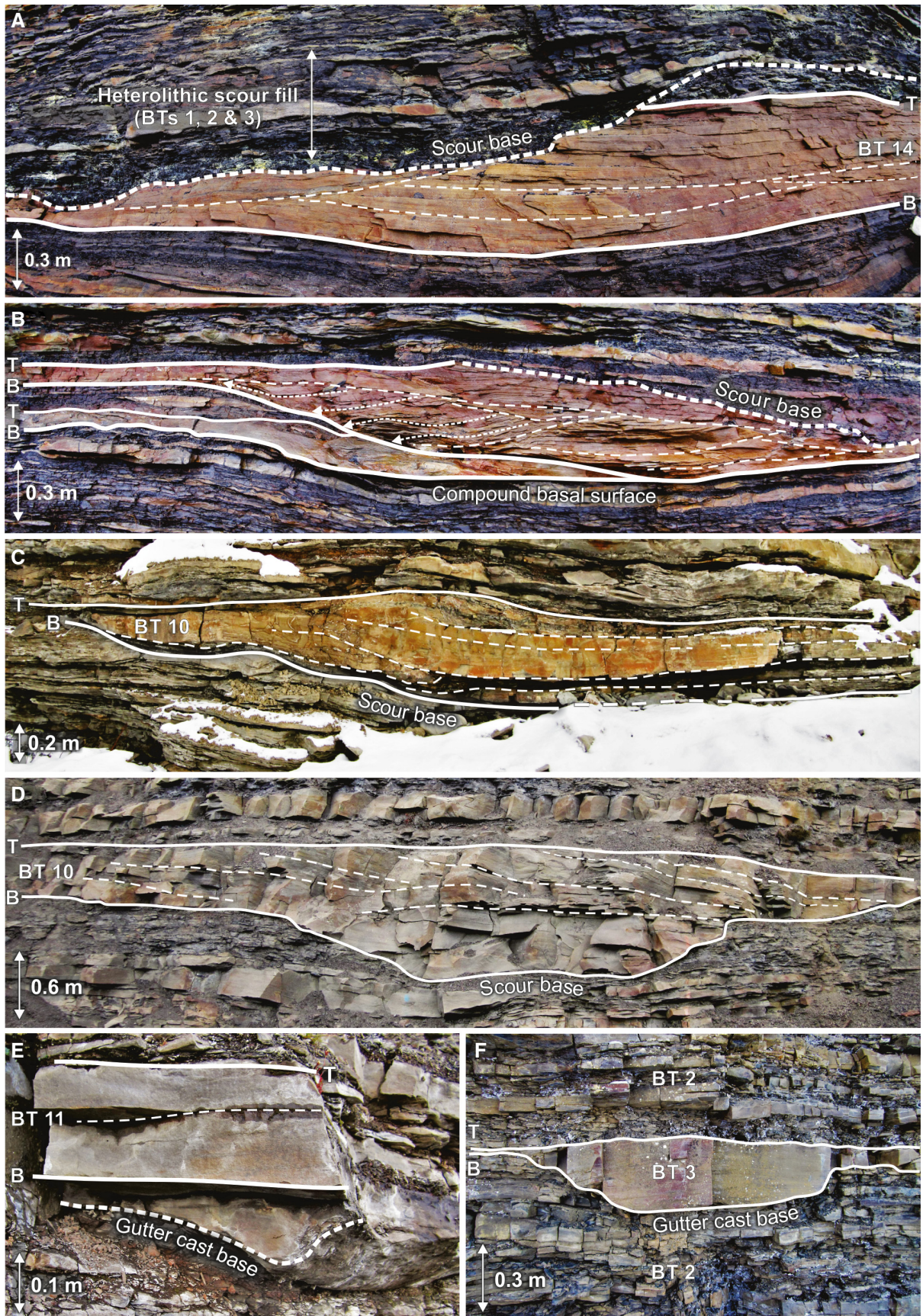


**Fig. 13.** Photographs of scours and gutter casts observed in the lower (A) and (B) and middle (C) to (F) wedges. (A) A several decimetre-deep scour (base marked by the thick stippled line) cutting into an underlying storm bed (of BT 14). Note the heterolithic scour infill consisting of BT 1 to BT 3. (B) A scour (marked by the thick stippled line) cutting into a ‘compound’ hummocky sandstone body’ (cf. Jelby *et al.*, 2020) containing multiple truncations surfaces. Climbing and partly laterally accreted lamina sets onlap one of the truncation surfaces (indicated by stippled arrows), indicating that the hummocky body itself represents a scour-and-fill element. Both (A) and (B) are from the uppermost parasequence of the lower wedge at Bohemanflya. (C) and (D) show examples of metre-scale scours with infills consisting of low-angle laterally (or frontally) accreted lamina sets (i.e. BT 10; see Fig. 9) occurring in the middle wedge. (E) and (F) show examples of gutter casts occurring at the base of two different types of storm beds in the middle wedge. B: bed base, T: bed top.

Formation (Figs 5B and 6F). Lenticular-bedded, wave-ripple cross-laminated sandstones occur in the upper part (BT 2), marking a gradual transition (and coarsening upward) into facies association MW 2. Pyrite and siderite nodules are present. Previous studies report total organic carbon (TOC) contents up to 2.5% (Midtkandal *et al.*, 2016; Grundvåg *et al.*, 2019). The upper shale unit is more than 100 m thick in some sections (for example, the Innkjegla Member in Fig. 6A and H) and generally fines upward.

Facies association MW 2 (‘thin-bedded storm deposits’; Fig. 14) consists of thinly-bedded, lenticular to wavy-bedded, very fine to fine-grained sandstone beds and rhythmically interbedded mudstones, together forming sheet-like heterolithic units. The sandstone beds display abundant isotropic HCS, and combined flow to wave ripple cross-laminations (BT 2 and BT 3; Figs 9 and 11A). Birkenmajer (1966) recorded bimodal palaeocurrent directions within these sandstones. Less common are normally-graded, sharp-based, gravel-rich sandstones beds displaying PPL, QPL, SCS and various types of climbing ripple sets (BT 4 to BT 7; Figs 9 and 11B). Decimetre-scale gutter casts occur rarely (BT 3; Fig. 13F). MW 2 commonly alternates with MW 3 or is sharply overlain by MW 4.

Facies association MW 3 (‘medium-bedded storm deposits with scours’; Fig. 14) comprises sheet-like heterolithic sandstone units consisting of thin to medium-bedded, lenticular to wavy-bedded, very fine to fine-grained sandstone beds exhibiting isotropic and (subordinate) anisotropic HCS and wave-rippled tops (BT 3, BT 9, BT 12 and BT 13; Fig. 11D and E). Lithic conglomerates and combined flow ripple cross-lamination occur (for example, BT 7; Fig. 11B). In many places, up to several metres wide and several decimetres deep sandstone-filled scours incise the underlying heterolithics (BT 10, Figs 6G, 9 and 13D). The scour infill is in many cases laterally (or frontally) accreted, onlapping

the basal scour surface (Fig. 13D). Decimetre-scale gutter casts occur frequently at the base of many beds (for example, BT 11; Fig. 13E). MW 3 typically occurs in the uppermost part of the Dalkjegla Member at the transition with the mudstone-dominated Innkjegla Member (i.e. the upper shale unit of MW 1; Figs 6A, 6G and 15C). MW 3 can be traced laterally up-dip into sandstone-dominated strata consisting of MW 2 and MW 4 (Fig. 15C, compare the inferred distal Ba-section with the up-dip Lo-section).

Facies association MW 4 (‘thick-bedded storm deposits’; Fig. 14) consists of up to several metres thick, amalgamated, tabular-shaped strata including thick-bedded, very fine to medium-grained sandstones exhibiting isotropic HCS to PPS, and wave-rippled bed tops (BT 17 and BT 18; Figs 9 and 11H). Locally, up to 1.5 m thick and several tens of metres long sandstone bodies with laterally thickening–thinning geometries occur (BT 16; Figs 9 and 11G). Internally, these bodies display a compound architecture with shingled, tapered and sigmoidal-shaped beds separated by (dip) conformable discontinuity surfaces. PPS, QPL and isotropic to anisotropic HCS occur within these bodies. MW 4 typically alternates with or caps heterolithic units consisting of MW 2.

Facies association MW 5 (‘trough cross-bedded sandstone’; Fig. 14) is characterized by tabular and amalgamated medium to coarse-grained sandstone beds displaying trough cross-bedding, PPS and occasional wave-ripple cross-lamination (BT 19; Figs 9 and 11I). MW 5 typically caps MW 4 deposits and is confined to the two or three lowermost parasequences of the middle wedge in the north-western part of the outcrop belt (for example, in the Festningen section shown in Fig. 6A and C, see Fig. 2B for location).

*Interpretation.* Based on the finely laminated character, mudstones of MW 1 are attributed to deposition from suspension settling in a low-energy, offshore environment, generally below

storm-wave base. The presence of lenticular-bedded sandstones with wave-ripple cross-lamination indicates minor storm influence and shallowing of the shelf. The sparse bioturbation, pyrite nodules, dark colour, and relatively high TOC content, indicate that the lower shale unit was deposited under dysoxic–anoxic conditions (Grundvåg *et al.*, 2019). Previous studies have recorded the Aptian oceanic anoxic event (OAE1a) in the lower shale unit (Midtkandal *et al.*, 2016), and demonstrated that it was deposited during an early Aptian regional flooding event, which drowned the Helvetiafjellet Formation delta plain (Grundvåg *et al.*, 2017, 2019). The fining-upward trend and great thickness (>100 m) of the upper shale unit points to gradual deepening of the shelf through time.

Based on the heterolithic character and dominance of sedimentary structures generated by oscillatory and oscillatory-dominated combined flow (for example, isotropic HCS and combined flow to wave-ripple cross-lamination), MW 2 is interpreted to represent storm-dominated offshore transition zone deposits. Bi-modal palaeocurrent directions within the lenticular-bedded sandstones suggest some tidal influence (Birkenmajer, 1966). Normally-graded, sharp-based, gravel-rich beds displaying climbing combined flow ripples suggest deposition by wave-modified turbidity currents (e.g. Myrow *et al.*, 2002). Because of the many sedimentological similarities to MW 2 (for example, non-amalgamated sandstone beds displaying isotropic HCS; Fig. 14), a storm-dominated offshore transition zone depositional setting is also suggested for MW 3. However, the abundance of scours and gutter casts in the MW 3 deposits, points to an offshore transition zone frequently eroded by powerful, offshore-directed, storm-generated flows (Eide *et al.*, 2015; Collins *et al.*, 2017; Olaussen *et al.*, 2018). The up-dip transition into MW 2 and MW 4, suggests that MW 3 represents a distal, offshore extension of these lower shoreface to offshore transition deposits (Fig. 15C).

The presence of lithic conglomerates at the base of some storm beds (BT 7; Figs 9 and 11B) in the MW 3 deposits is attributed to rare storm events eroding coastal areas and generating strong offshore-directed currents capable of transporting gravel as bedload into deeper waters (possibly by high-density, wave-modified turbidity currents). The associated scours in MW 3 may have confined and enhanced these currents.

The thick-bedded character of MW 4 and the dominance of amalgamated, isotropic HCS

sandstone beds, suggest deposition in a storm-dominated lower shoreface or delta front environment (Van Wagoner *et al.*, 1990; Hampson & Storms, 2003; Bowman & Johnson, 2014; Eide *et al.*, 2015). The compound hummocky bodies internally displaying shingled, sigmoidal-shaped beds (i.e. BT 16; Fig. 9) represent large-scale migrating bedforms generated by storm-wave and tidal current interactions in the nearshore environment (e.g. Johnson, 1977; Tinterri, 2011).

The coarse-grained and trough cross-bedded nature of MW 5 suggests deposition by migrating 3D dunes possibly induced by breaking waves, in an upper shoreface setting. The interbedded horizons displaying PPS and wave-ripple cross-lamination record wave-reworking under fluctuating wave velocities. The local distribution of MW 5 suggests proximity to a shoreline in the west to north-west (Grundvåg *et al.*, 2019).

#### *Facies associations of the upper wedge*

**Description.** Facies association UW 1 ('thin-bedded storm deposits'; Fig. 14) has a heterolithic character and consists of siltstones, abundant thin-bedded (<10 cm), lenticular to wavy-bedded sandstones (BT 1 to BT 3; Figs 9, 12A and 12B) and thin mudstone interbeds. The sandstone–mudstone ratio varies from 70:30 to 30:70, but generally sandstone comprises more than 50% in any measured section (Fig. 12B). The sandstone content and bed thickness increase upward into the overlying deposits of UW 2 ('thin to medium-bedded storm deposits'). The lenticular-bedded sandstones commonly display wave-ripple cross-lamination. Sandstone-filled scours containing basal lags of bivalve and ammonite fragments occur sporadically (BT 8; Figs 9, 12E and 12F), incising into the underlying heterolithics. UW 1 commonly alternates with UW 2.

Facies association UW 2 ('thin to medium-bedded storm deposits'; Fig. 14) is characterized by stacks of non-amalgamated, medium-bedded, isotropic HCS sandstone beds (BT 13), or small-scale (<3 m thick) thickening-upward and coarsening-upward units (Fig. 12C). The lower part of these units is thin-bedded and heterolithic (consisting of BT 2 and BT 3; Fig. 12C), whereas their upper part is characterized by medium-bedded, non-amalgamated to amalgamated isotropic HCS sandstone beds (BT 9 or BT 13; Figs 7A, 7B and 12C). Bivalve and ammonite fragments are present. UW 2 is typically sharply overlain by UW 3.

Facies association UW 3 ('thick-bedded storm deposits'; Fig. 14) consists of thick-bedded

isotropic HCS sandstone beds (BT 17 and BT 18), which stack to form tabular and amalgamated units up to 6 m thick (Figs 7B and 16A). Wave-ripple cross-lamination, discontinuous sideritic mudstone interbeds, (sideritic) mudstone rip-up clasts, various shell fragments and petrified wood material occur locally (Fig. 7B).

*Interpretation.* Based on the abundance of thin-bedded sandstones displaying isotropic HCS and wave-ripple cross-lamination, UW 1 is attributed to deposition in a storm-dominated shelf environment frequently influenced by storm-generated oscillatory flows (Fig. 17). The local occurrence of shell-rich, sandstone-filled scours records rare erosional events and subsequent deposition by storm-generated, turbulent combined flows (Pérez-López, 2001). The heterolithic and thin-bedded nature of UW 1 may reflect deposition in distal or deeper shelf settings or record longer periods of weaker, but still frequent storm activity with the seafloor mostly positioned above SWB (Dott & Bourgeois, 1982; Brenchley *et al.*, 1986; Runkel *et al.*, 2007).

The medium-bedded, isotropic HCS sandstone beds of UW 2 indicate deposition by storm-generated oscillatory-dominated flows. The small-scale upward coarsening units may record the distal-most part of prograding shore-attached sediment tongues, shallowing of the offshore environment, higher sand influx, or deposition and reworking by progressively larger and stronger storm-waves (Aigner & Reineck, 1982; Dott & Bourgeois, 1982). Water depths are difficult to assess, but bivalve and ammonite fragments suggest an open marine shelf environment for UW 2.

Based on the abundance of isotropic HCS, and the thick-bedded and amalgamated character of the sandstone beds, UW 3 is attributed to deposition in a storm-dominated lower shoreface to innermost shelf environment experiencing frequent storm-related sediment reworking (Fig. 17; Aigner & Reineck, 1982; Dott & Bourgeois, 1982; Brenchley *et al.*, 1993; Hampson & Storms, 2003). Interbedded sideritic mudstones represent deposition during fair-weather conditions, whereas the associated sideritic mudstone rip-up clasts indicate local erosion. Siderite does not form syn-depositionally in normal marine environments, but is commonly linked to early diagenesis and reducing conditions involving organic-rich material containing moderate amounts of iron (Campbell & Campbell, 2018).

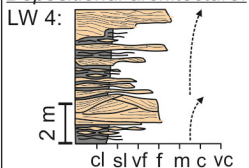
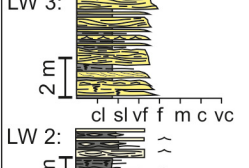
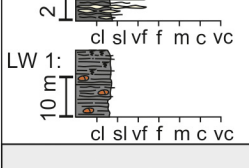
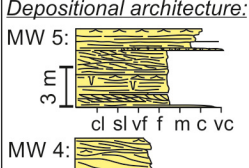
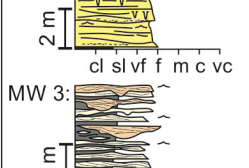
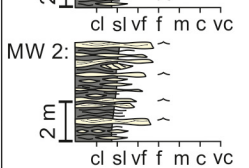
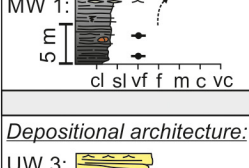
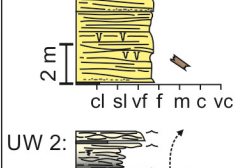
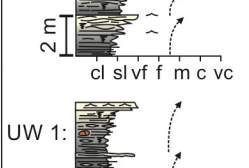
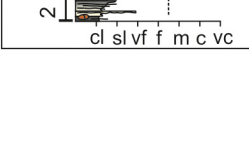
## Parasequence architecture and stacking patterns

The facies associations in each wedge typically stack to form *ca* 10 to 30 m thick, coarsening-upward and thickening-upward units, here referred to as parasequences (*sensu* Van Wagoner *et al.*, 1990; Figs 6 to 8 and 14 to 16). In a stacked series, parasequences are separated by marine flooding surfaces, which are identified by abrupt upward deepening or fining of facies. Whether the parasequences of this study represent true basin-wide units is difficult to assess due to outcrop limitations. However, for the purpose of defining large-scale stacking trends within the wedges, the classical parasequence terminology of Van Wagoner *et al.* (1990) is fully applicable.

Internally, the parasequences may contain several smaller-scale upward-coarsening units here referred to as parasequence bed-sets (for example, Fig. 12C and D). A bed-set consists of a series of genetically related beds bounded atop by a bed-set surface of minor erosion or non-deposition (Van Wagoner *et al.*, 1990; Hampson & Storms, 2003). Outcrop limitations make it difficult to establish whether or not some of the thicker bed-sets instead represent parasequences.

### *Parasequences of the lower wedge*

*Description.* Facies association LW 1 ('mudstone-dominated deposits'; Fig. 14) forms a *ca* 200 to 300 m thick mudstone-dominated succession in the lower part of the wedge (assigned to the Wimanfjellet Member; Figs 5A, 6A and 6D). In the upper 50 to 100 m thick sandstone-rich part of the wedge, facies associations LW 2 ('thin to medium-bedded storm deposits') and LW 3 ('thick-bedded storm deposits') repeatedly stack to form a series of coarsening-upward and thickening-upward units conforming to parasequences (*sensu* Van Wagoner *et al.*, 1990; Figs 3C, 6A, 6B and 6E). None of the parasequences grade upward into upper shoreface or foreshore facies. The parasequences are arranged into a progradational parasequence set (*sensu* Van Wagoner *et al.*, 1990), which is most typically succeeded by a retrogradational parasequence set (Figs 5A and 6A). In the northernmost part of the study area, the retrogradational parasequence set is overlain by a relatively thin (<10 m) unit of renewed progradation (for example, Fig. 15A). Individual parasequences are heterolithic and relatively thin (generally <15 m; Fig. 6B), and contain abundant isotropic HCS (for example, BT 3 and BT 13; Fig. 14; Jelby *et al.*,

Facies associations of the lower wedge (LW 1 - LW 4)			
<i>Depositional architecture:</i>	<i>Bed types:</i>	<i>Description:</i>	<i>Depositional environment:</i>
LW 4: 	B <sub>1</sub> , BTs 3, 4, 5, 6, 12, 13, 14 and 15.	<i>'Heterolithic sandstone deposits with scours':</i> Heterolithic sandstone succession comprising stacked coarsening upward units. Metre-scale scour-and-fill features, gravel lenses, and tempestite beds displaying isotropic to anisotropic HCS, SCS and QPL are present.	Storm-dominated prodelta to distal delta front. Deposition and scouring by a variety of processes including oscillatory-dominated combined flows, hyperpycnal flows and wave-modified turbidity currents.
LW 3: 	BTs 3, 9, 12 (rare), 13 and 14 (rare).	<i>'Thick-bedded storm deposits':</i> Amalgamated to non-amalgamated, sandstone-dominated units mainly displaying isotropic HCS, WRCL and CFR. Anisotropic HCS and QPL occur locally.	Storm-dominated lower shoreface. Reworking and deposition by oscillatory flows, oscillatory-dominated combined flows, and rare wave-modified turbidity currents.
LW 2: 	BT 1 to BT 4 and BT 9.	<i>'Thin- to medium-bedded storm deposits':</i> Non-amalgamated tempestite beds displaying isotropic HCS and wave-rippled tops forming tabular-shaped, heterolithic sandstone units.	Storm-dominated offshore transition zone. Deposition by oscillatory-dominated combined flows and rare wave-modified turbidity currents.
LW 1: 	B <sub>1</sub> , B <sub>2</sub> , B <sub>3</sub> , BTs 1 and 2 (rare).	<i>'Mudstone-dominated deposits':</i> Up to several tens of metres thick, laterally extensive, sheet-like successions consisting of laminated to bioturbated mudstone.	Offshore. Mud and silt deposition predominantly by suspension settling and low-density turbidity currents below SWB.
Facies associations of the middle wedge (MW 1 - MW 5)			
<i>Depositional architecture:</i>	<i>Bed types:</i>	<i>Description:</i>	<i>Depositional environment:</i>
MW 5: 	BT 19 and 18 (rare).	<i>'Trough cross-bedded sandstone':</i> Amalgamated, medium- to coarse-grained sandstone units displaying trough cross-stratification, PPS, and WRCL.	Upper shoreface. Deposition by unidirectional currents induced by breaking waves, eventually forming 3D dunes and upper plane beds.
MW 4: 	BTs 2 (thin interbeds), 16, 17 and 18.	<i>'Thick-bedded storm deposits':</i> Several metres thick, amalgamated sandstone successions dominated by isotropic HCS. Large-scale, compound hummocky bodies with lateral accreted sigmoidal beds occur in places (BT 16).	Storm-dominated lower shoreface or delta front. The compound hummocky bodies with lateral accreted sigmoidal beds represent storm-generated and tidally-modulated large-scale bedforms.
MW 3: 	BTs 3, 7, 9, 10, 11, 12, 13 and 14.	<i>'Medium-bedded storm deposits with scours':</i> Sheet-like, heterolithic units consisting of lenticular- to wavy-bedded, isotropic to anisotropic HCS sandstone beds. Metre-scale scours and gutter casts occur locally.	Erosive offshore transition zone (middle to distal shelf). Frequent scouring by powerful, storm-generated, possibly tidally-enhanced, combined flows.
MW 2: 	BTs 2, 3, 4, 5 (rare), 6 (rare), 7 (very rare)	<i>'Thin-bedded storm deposits':</i> Tabular-shaped, heterolithic units dominated by thin-, lenticular- to wavy-bedded sandstones. HCS and CFR to WRCL are common.	Offshore transition zone. Deposition by waning, storm-generated combined to oscillatory-dominated combined flows, and by rare wave-modified turbidity currents.
MW 1: 	B <sub>1</sub> , B <sub>2</sub> , B <sub>3</sub> , BTs 1 and 2 (rare).	<i>'Mudstone-dominated deposits':</i> Finely laminated, locally dark-coloured, mudstone successions with rare sandstone lenses. Siderite concretions occur.	Offshore. Dominantly suspension settling below SWB. Periodically oxygen deficient bottom conditions and slow deposition.
Facies associations of the upper wedge (UW 1 - UW 3)			
<i>Depositional architecture:</i>	<i>Bed types:</i>	<i>Description:</i>	<i>Depositional environment:</i>
UW 3: 	BTs 17, 18, and BT 2 (as thin interbeds).	<i>'Thick-bedded storm deposits':</i> Up to 6 m thick, amalgamated sandstone units dominated by isotropic HCS. Erosive sharp to undulating bed bases, WRCL, wave-rippled bed tops, mudstone rip-up clasts, and abundant fossil wood material are present.	Storm-dominated lower shoreface-innermost shelf. Frequent reworking and sediment re-distribution by storm waves. Abundant wood may indicate proximity to a fluvial feeder system.
UW 2: 	BTs 1, 2, 3, 9, 13, 17 (rare).	<i>'Thin- to medium-bedded storm deposits':</i> Up to 5 m thick heterolithic, upward coarsening units with thin and lenticular-bedded lower parts passing upward into thicker, isotropic HCS beds. Loaded bases and wave rippled bed tops occur locally.	Storm-dominated offshore transition (middle shelf). Deposition dominated by oscillatory flows. The upward coarsening cycles indicate repeated progradation or shallowing of the offshore transition zone.
UW 1:	B <sub>1</sub> (thin interbeds), BTs 1, 2, 3, 8 (rare), 9 (rare).	<i>'Thin-bedded storm deposits':</i> Several metres thick, lenticular- to wavy-bedded heterolithic sandstone units. Isotropic HCS and WRCL occur. Lags of bivalve shells are present in rare scour infills (i.e. BT 8).	Offshore shelf. Shallow water depths with seafloor above SWB, promoting frequent storm deposition. Shell lags indicate winnowing of local shell banks.

2020). There is a clear proximal to distal trend from the north-west to the south-east along the outcrop belt with parasequences fining and thinning towards the east and ESE (Figs 3C and 4B; Dypvik *et al.*, 1991a; Jelby *et al.*, 2020).

The uppermost progradational parasequence of the lower wedge is dominated by facies association LW 4 ('heterolithic sandstone deposits with scours') across large parts of the study area, and is characterized by abundant scour-and-fill features, gutter casts, and sandstone beds exhibiting SCS, isotropic to anisotropic HCS and current ripple to combined flow ripple cross-lamination (Figs 14 and 15C). Published palaeocurrent data for foreset dip-azimuths of the current ripple cross-lamination and anisotropic HCS range between west, south-west, south, south-east and east, with a SSE-trend dominating in many locations (Dypvik *et al.*, 1991b; Grundvåg *et al.*, 2019; Jelby *et al.*, 2020). Parting lineations and gutter casts are generally north-west/south-east-oriented, whereas wave-ripple crest strikes record an east-west to south-west/north-east-dominating trend (Grundvåg *et al.*, 2019; Jelby *et al.*, 2020).

**Interpretation.** The shale-dominated part of the lower wedge consisting of LW 1, suggests accumulation in relatively deep shelfal waters with the basin floor positioned below SWB (Figs 3C, 4B and 18A). The parasequences in the upper part of the wedge record a progradational phase, succeeded by a retrogradational phase (Figs 3C, 5A and 6A), which is locally finalized by a progradational phase of the uppermost deltaic parasequence (consisting of LW 4 deposits). The dominance of isotropic HCS sandstone beds and wave ripple cross-lamination indicates a storm-dominated shoreface to delta front origin for the parasequences (Van Wagoner *et al.*, 1990; Cross & Lessenger, 1997; Hampson & Storms, 2003).

Previous palaeogeographic reconstructions indicate a SSW–NNE-oriented shoreline building basinward in a south-east to ESE direction, roughly coincident with the progradation direction of the overlying fluvio-deltaic Helvetiafjellet Formation (Fig. 4B; Midtkandal & Nystuen, 2009; Jelby *et al.*, 2020).

The increased abundance of medium to coarse-grained sandstone beds locally exhibiting SCS (BTs 14 to 15) and gutter casts, as well as the occasional presence of anisotropic HCS sandstone beds (BT 12), combined flow-ripple to current-ripple cross-lamination, and the heterolithic to sandstone-filled scours indicate a prodelta to delta front origin for the uppermost parasequence (i.e. LW 4; Figs 15A and 18A). This parasequence may reflect the earliest stage of the forced regression that later drove the overlying Helvetiafjellet Formation delta system to the south-east (Fig. 4C; Nemec *et al.*, 1988; Grundvåg *et al.*, 2019; Jelby *et al.*, 2020). The storm beds recorded in these prodelta to delta front deposits suggest deposition by various basinward-directed combined flows and strong turbulent, unidirectional flows (Figs 9, 14, 15A and 18A). Thus, the proximity to an approaching fluvio-deltaic system exerted a strong control on the depositional processes responsible for the observed storm-bed variability.

#### *Parasequences of the middle wedge*

**Description.** The lower part of the middle wedge is characterized by a regionally extensive 10 to 30 m thick, lower Aptian shale unit consisting of facies association MW 1 (Fig. 15C). The shale separates the middle wedge from the underlying Helvetiafjellet Formation (Fig. 2D; Midtkandal *et al.*, 2016; Grundvåg *et al.*, 2017, 2019). Above the shale, a *ca* 100 m thick and regionally extensive sandstone-dominated succession occurs. Within this succession, facies associations MW 2 ('thin-bedded storm deposits') and MW 4 ('thick-bedded storm deposits') repeatedly stack to form coarsening-upward and thickening-upward units conforming to parasequences (Figs 6A, 6B, 14 and 15C). The lowermost two to three parasequences are progradationally stacked and typically more sandstone-dominated and amalgamated than the following parasequences, thus corresponding to a progradational parasequence set (Fig. 6C). In the north-western part of the study area, the lowermost parasequences are more coarse-grained consisting of MW 5 ('trough cross-

**Fig. 14.** Schematic summary of the various facies associations recognized in the investigated wedges. Facies associations LW 1 to LW 4 occur in the lower wedge, facies associations MW 1 to MW 5 occur in the middle wedge, whereas facies associations UW 1 to UW 3 is restricted to the upper wedge. CFR: combined flow ripple cross-lamination, HCS: hummocky cross-stratification, PPS: plane parallel stratification, QPL: quasi-planar lamination, SCS: swaley cross-stratification, SWB: storm-wave base, WRCL: wave ripple cross-lamination.

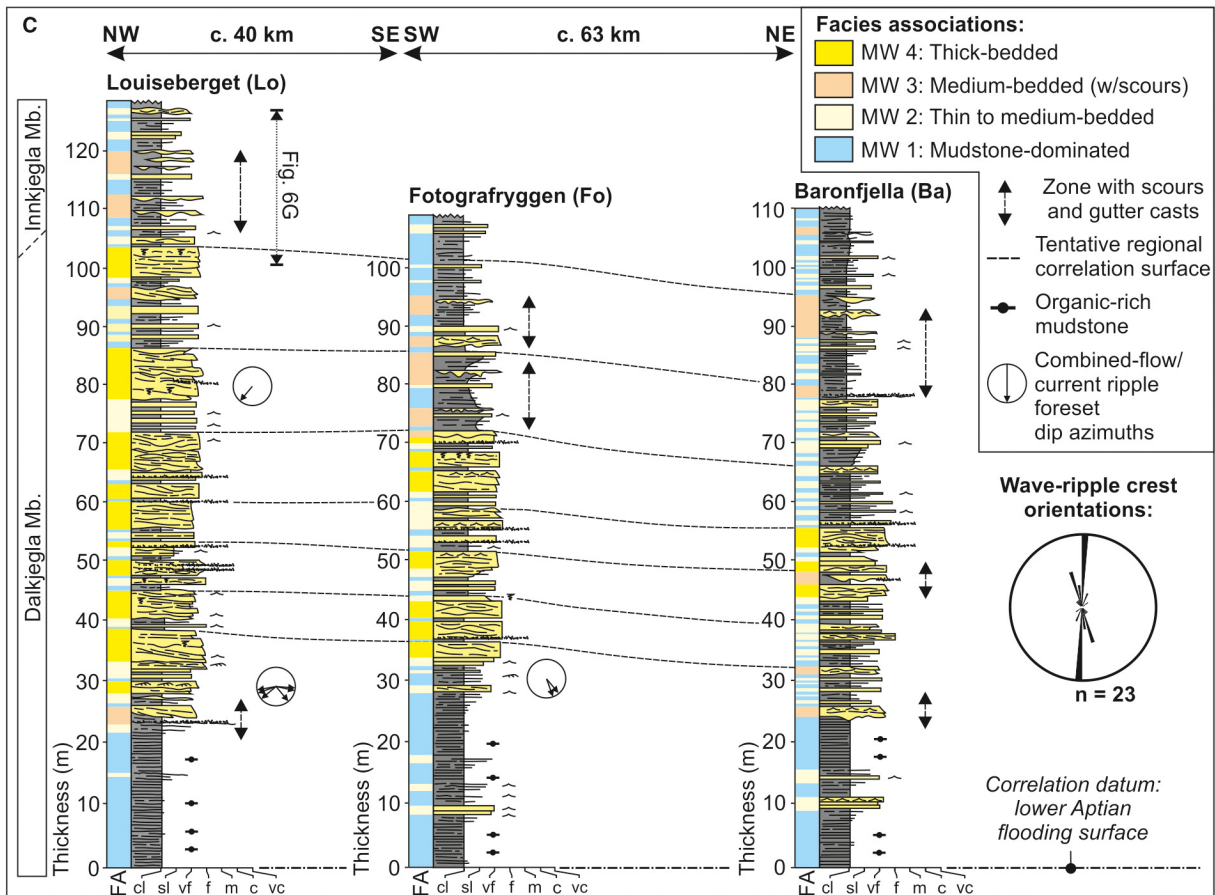
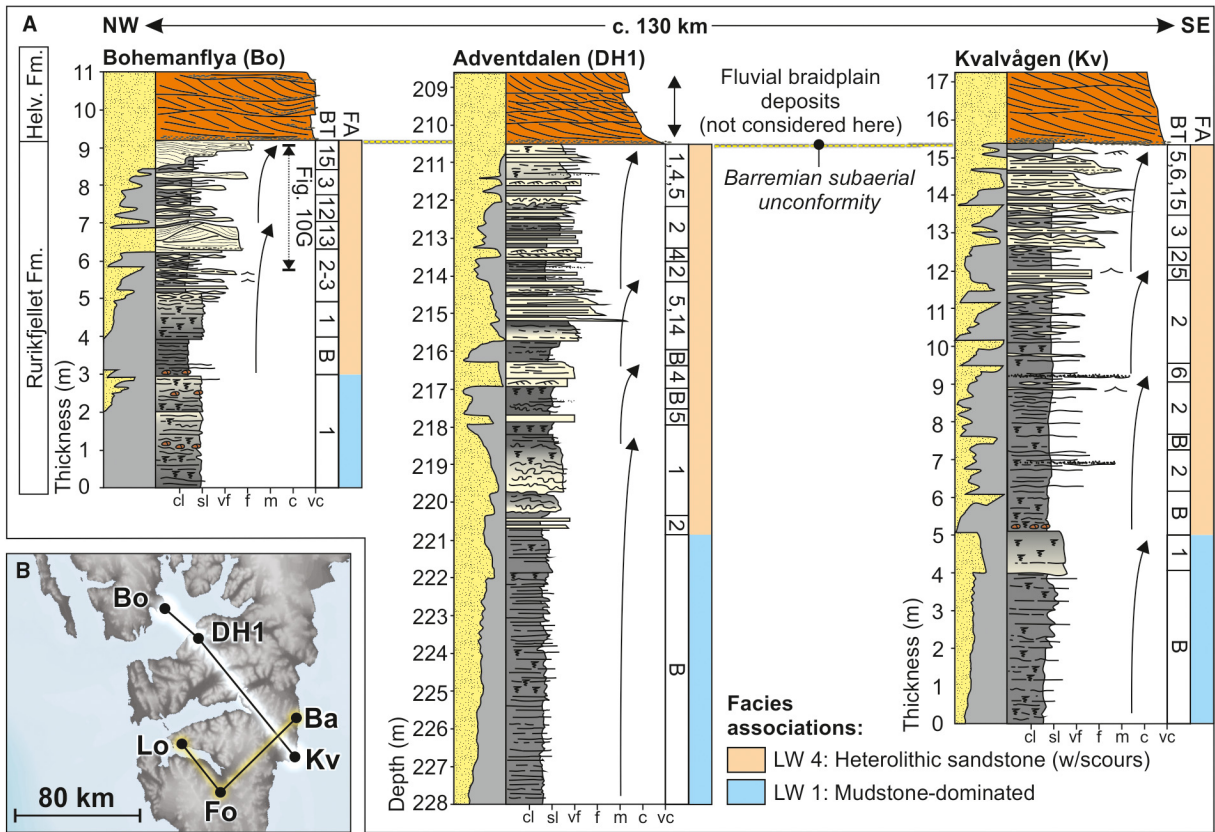


**Fig. 15.** A selection of measured sections of the lower and middle wedges. (A) Detailed sedimentological logs through the uppermost parasequence of the lower wedge from proximal (Bo-section) to intermediate (DH1) and distal (Kv-section) parts of the outcrop window (*sensu* Jelby *et al.*, 2020). The uppermost parasequence of the lower wedge comprises a wide range of storm-beds and scours (for example bed types 4, 5, 6, 12, 14, 15; see Fig. 9 for details) suggesting fluvio-deltaic influence (facies association LW 4) and possibly coupled storm–flood interactions. Location of sections is given in (B). (C) Detailed logs of the middle wedge illustrating the vertical and lateral distribution of facies associations from inferred proximal (Lo-section) to intermediate (Fo-section) and distal (Ba-section) parts of the outcrop window. The tentative semi-regional correlation indicates that the heterolithic units containing abundant scours and gutter casts (facies association MW 3) represent a distal facies development of the otherwise sandstone-dominated parasequences (consisting of recurrent stacks of facies associations MW 1, MW 2 and MW 4). Legend is given in Fig. 6I.

bedded sandstone’) deposits in their upper part (for example, in the Festningen section, Fig. 6C). The succeeding parasequences are typically more heterolithic and they commonly thicken and fine upward (Fig. 6A, 6C and 15C), thus representing a retrogradational parasequence set.

Abundant scours and gutter casts characterize MW 3 (‘medium-bedded sandstones with scours’), which occur locally within some parasequences. Stratigraphically, MW 3 occurs most commonly in the upper part of the lower wedge in the transition zone between the sandstone-dominated Dalkjegla Member and the overlying shale-dominated Innkjegla Member. In addition, MW 3 is a common feature within heterolithic parasequences in sections located along the east coast. These parasequences apparently become more sandstone-rich and amalgamated up-dip (Fig. 15C, contrast sections Ba and Lo).

The low-angle foreset laminae in anisotropic HCS sandstone beds (BT 12) within the upper part of the wedge dip towards the west and south-west (Nøttvedt & Kreisa, 1987). A large spread is, however, evident when measurements from multiple outcrop locations are included, ranging from east, south-east, south, south-west and west (Birkenmajer, 1966; Grundvåg *et al.*, 2019). In the deposits of MW 3, gutter casts (in BT 11 and BT 14) and the axis of the many scours (BT 10) are oriented in a north-west/south-east direction, whereas the foresets of current ripple cross-laminated beds (for example, BT 4 and BT 7) dip towards the east and south-east. Wave-ripple crests generally strike in a north–south to north-east/south-west direction (Birkenmajer, 1966; Maher & Shuster, 2007; Grundvåg *et al.*, 2019).

*Interpretation.* The lower shale unit (consisting of MW 1) accumulated during an early Aptian regional flooding event that drowned the Helvetiafjellet Formation delta top and re-established

marine shelf conditions across Svalbard (Midtkandal *et al.*, 2016; Grundvåg *et al.*, 2017, 2019; Figs 2D and 4D). The succeeding progradationally stacked parasequences, record renewed shoreline progradation onto the storm-dominated shallow shelf (Figs 4E, 5B, 6A and 6F). The coarse-grained deposits with trough cross-bedded sandstones (MW 5, interpreted to represent upper shoreface deposits; Fig. 14) in the parasequences in the north-western part of the outcrop belt, indicate the presence of a shoreline to the north-west. The heterolithic parasequences in eastern Spitsbergen are thus interpreted to reflect more distal environments (Figs 3A, 4E and 15C). Published palaeogeographic reconstructions indicate a west–east, north-west/south-east, or south-west/north-east-oriented lobate palaeoshoreline, consistent with the overall northward retreat of the associated fluvio-deltaic system of the Helvetiafjellet Formation (Fig. 4C and D; Birkenmajer, 1966; Steel & Worsley, 1984; Maher *et al.*, 2004; Mutrux *et al.*, 2008; Grundvåg *et al.*, 2019). The retrogradationally-stacked parasequences confirm a long-term (i.e. several hundreds of thousands to a few millions of years) transgressive development for the middle wedge. As such, the upward-thickening and upward-fining of parasequences suggest deposition in increasingly deeper waters.

Based on the dominance of storm-dominated and wave-dominated structures (in basically all of the facies associations; Fig. 14), the middle wedge is generally interpreted as a storm-dominated shoreface – inner shelf system. It is suggested here that the middle wedge records a second-order regressive pulse of the retreating Helvetiafjellet Formation delta, thus representing its lateral distal equivalent (Figs 2D and 4E). The laterally extensive distribution of the middle wedge (for example, Figs 3A, 3B and 15C) relate to the low-angle facies belts of the retrogradationally stacked parasequences. Landward-stepping wedges typically transit across

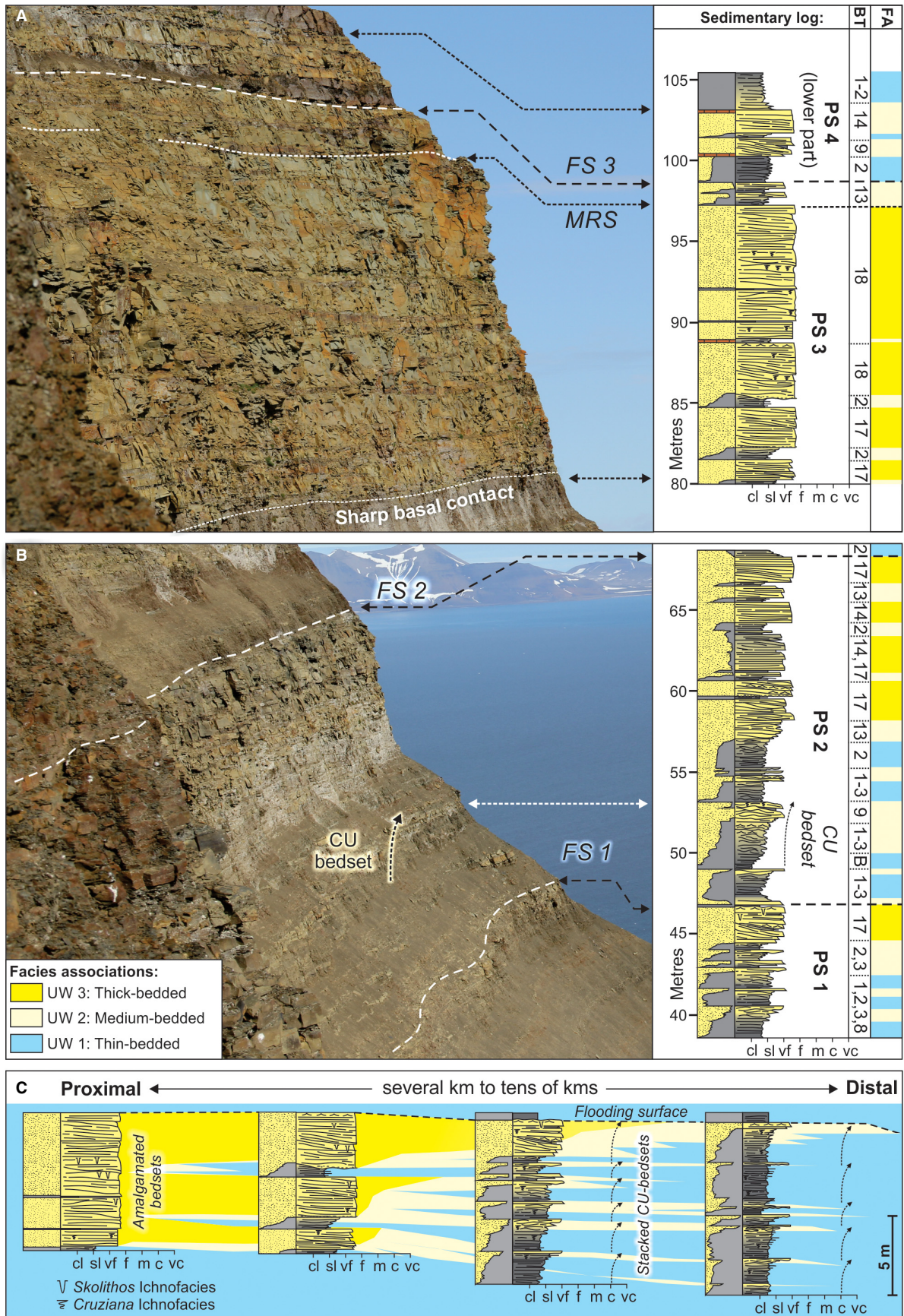


**Fig. 16.** Outcrop photographs and accompanying sedimentological logs of PS 1 to PS 3 of the upper wedge at Schönrockfjellet. (A) PS 3 consist of thick-bedded and amalgamated tempestite beds (that is BT 17 and BT 18 comprising facies association UW 3; Fig. 14), suggesting storm deposition in a proximal shelf environment. PS 1 and PS 2 have thin-bedded, heterolithic lower parts and display clear coarsening-upward and thickening-upward trends. (C) Schematic illustration of an idealized parasequence based on the observed vertical distribution of facies associations (UW 1 to UW 3; Fig. 14) and parasequence stacking (for example PS 1 to PS 3). Legend is given in Fig. 6I.

shallow, gently sloping shelves constituted by the transgressed platform of the underlying unit. As a result, their seafloors are commonly positioned above the effective wave base (e.g. Cross & Lessenger, 1997). The result is that sand is being dominantly removed from the shoreface zone and transported across the shelf to form laterally extensive, sand-dominated facies belts stretching several tens of kilometres from the actual shoreline (e.g. Runkel *et al.*, 2007; Plint, 2014; Jelby *et al.*, 2020).

Despite its regional extent and systematic parasequence stacking, it has previously been suggested that the middle wedge represents shore-detached offshore bars or barrier complexes which accumulated in a storm-dominated shelf setting (Maher *et al.*, 2004; Maher & Shuster, 2007; Mutrux *et al.*, 2008). However, such interpretations are not favoured here.

The presence of anisotropic HCS, gutter casts and sandstone-filled scours have previously been interpreted to record strong east-west-directed unidirectional flows during storms,

roughly paralleling an inferred linear palaeoshoreline to the north (Fig. 4E; Nøttvedt & Kreisa, 1987; Maher *et al.*, 2004). The strong westward flows may have been associated with geostrophic flows and/or the predominantly westward wind direction in the Northern Hemisphere caused by the polar easterlies (Maher & Shuster, 2007). However, some palaeoclimatic studies have questioned the presence of this polar wind system in the Cretaceous 'greenhouse' world (e.g. Hay, 2009). Further, this interpretation is not consistent with regional palaeocurrent measurements which display a large spread in an overall basinward direction (Birkenmajer, 1966; Grundvåg *et al.*, 2019). Most palaeogeographic reconstructions for the Dalkjegla Member favour the presence of a roughly east-west-oriented, lobate palaeo-shoreline (Birkenmajer, 1966; Steel & Worsley, 1984; Grundvåg *et al.*, 2017; Fig. 4E). Such a lobate coastline would thus give rise to local differences in depositional dips and consequently a wide spread in the direction of basinward-

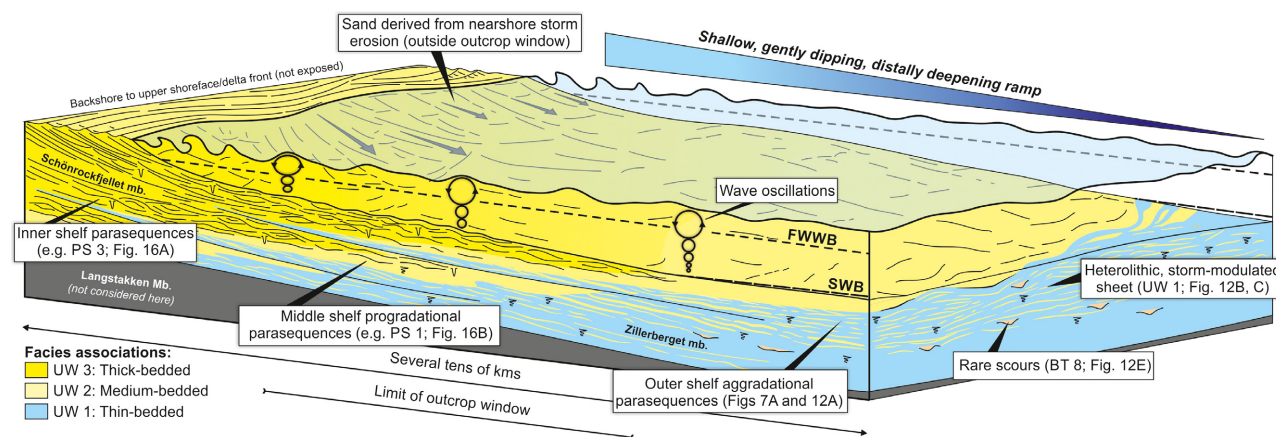


**Fig. 17.** Depositional model for the upper wedge. Due to the shallow, low-angle ramp setting, most of the seafloor was predominantly positioned above storm-wave base (SWB), causing frequent storm-wave reworking of sediments derived from nearshore areas, which erased the signature of other potential transport processes. The position of the SWB further promoted the accumulation of lenticular and thin-bedded storm beds in the distal and deeper parts of the shelf, forming laterally extensive tempestite sand sheets across large parts of the shelf. The observed depositional architecture of the wedge suggests that the parasequences and the associated tempestite sheets were shore-attached rather than representing an offshore bar complex. FWWB: Fair-weather wave base.

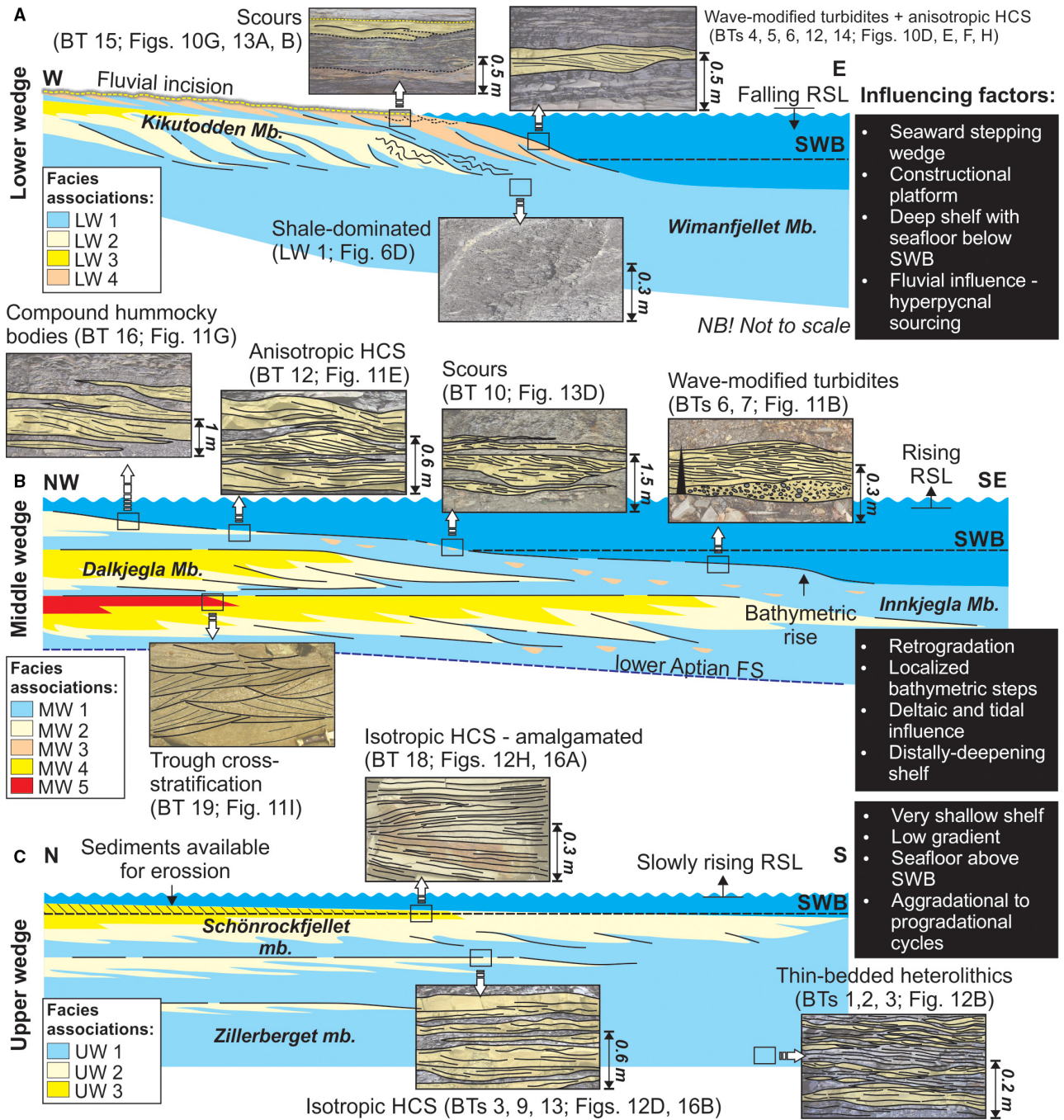


**Fig. 18.** Conceptual model illustrating the main factors influencing storm-bed variability in the investigated wedges. (A) The lower wedge (the Rurikfjellet Formation) exhibits a large-scale, predominantly coarsening-upward trend with progradationally stacked parasequences overlying a thick mudstone succession. Because the lower wedge built into deeper shelf waters, it was characterized by comparably steeper depositional dips than the middle and upper wedges. Scours, wave-modified turbidites, and a few tempestite beds exhibiting anisotropic hummocky cross-stratification (HCS) mainly occur in the uppermost, deltaic part of the wedge. (B) The middle wedge (the Dalkjegla Member) exhibits an overall landward-stepping architecture. Localized bathymetric steps and increased depositional dips in the distal parts of retrogradationally stacked parasequences enhanced by bypassing currents, and promoted scouring and the generation of migrating bedforms (i.e. anisotropic hummocks). (C) The upper wedge (the Schönrockfjellet and Zillerberget members) prograded onto a shallow, gently sloping shelf. The basin floor was in all places positioned above storm wave base (SWB), resulting in severe storm-wave reworking and the dominance of tempestite beds exhibiting isotropic HCS. See Fig. 9 for bed type details and Fig. 14 for facies-association characteristics.

directed flows. This is consistent with published palaeocurrents towards the west, south-west, south, south-east and east (Birkenmajer, 1966; Nøttvedt & Kreisa, 1987; Grundvåg *et al.*, 2019).

The local occurrence of heterolithic deposits displaying bimodal palaeocurrent indicators (in MW 2; e.g. Birkenmajer, 1966), and the local occurrence of shingled, compound hummocky sandstone bodies (BT 16; Fig. 9), suggest some tidal influence during deposition of the middle wedge. Various tidal facies also occur frequently in the underlying fluvio-deltaic Helvetiafjellet Formation (Gjelberg & Steel, 1995; Midtkandal & Nystuen, 2009), indicating that tidal currents influenced the palaeo-coastline and the inner shelf. Thus, it is possible that tidal currents directly influenced the formation of various-scale storm-generated bedforms (preserved as anisotropic HCS in BT 12 and compound hummocky beds of BT 16; Fig. 9) or enhanced the currents responsible for their generation (Vakarlov *et al.*, 2012; Basilici *et al.*, 2012b). In addition, it is suggested that tidal currents may have influenced the extent of the facies belts previously reported in the middle wedge (Grundvåg *et al.*, 2019). The combination of storm and tidal currents may result in extensive lateral redistribution of shelf sediments (Johnson, 1977).

Landward-stepping wedges comprising retrogradationally-stacked parasequences may commonly preserve bathymetric steps on the shelf. If a shoreface–shelf parasequence is rapidly transgressed, its steep front and platform break may be preserved, creating a localized bathymetric step (Cross & Lessenger, 1997; Eide *et al.*, 2015). Several studies have suggested that such steps may be instrumental in the development of scours and channels on the shelf, particularly if the succeeding parasequence progrades across the platform break of the preceding parasequence (Eide *et al.*, 2015). A similar concept, with bathymetric steps forming on the shelf at the platform break of retrogradationally stacked parasequences, may explain the stratigraphic and lateral occurrence of scours and gutter casts (MW 3) in the middle wedge (Figs 15C and 18B). Offshore-directed flows passing these breaks would surely increase in velocity and thus become more erosive.

#### *Parasequences of the upper wedge*

**Description.** In the upper wedge, UW 1 to UW 3 repeatedly stack to form up to 30 m thick coarsening-upward and thickening-upward successions conforming to parasequences bounded

atop by flooding surfaces that are marked by an increase in palaeo-water depth (*sensu* Van Wagoner *et al.*, 1990; Figs 7, 8 and 16). The most complete parasequences consist of thin-bedded storm deposits in their lower part (UW 1), grading upward via medium-bedded (UW 2) to thick-bedded (UW 3) storm deposits in their upper part (Fig. 16). The upper part of the wedge (i.e. the Schönrockfjellet member) comprises seven parasequences (PS 1 to PS 7) with the uppermost one being truncated by the regional Palaeogene unconformity (Figs 7A, 7B and 8). Except for this major regional hiatus, there is no indication of subaerial exposure in any of the other parasequences; nor proximal facies attributable to coastal plain, foreshore or upper shoreface environments. Within the limited lateral extent of the north-east/south-west-oriented outcrop, these parasequences have a tabular architecture (Fig. 8), and their lower part appears to split into vertically stacked coarsening-upward bed-sets characterized by thin to medium-bedded storm deposits (UW 2; Figs 7B, 8 and 12C). PS 1 to PS 3 exhibit a clear progradational stacking pattern with PS 3 having a sharp base and by far being the most amalgamated unit (Figs 7B, 8 and 16). PS 4 to PS 7 progressively thin upward in concert with a steady upward increase in interbedded mudstone (Fig. 7B).

The lower part of the upper wedge (i.e. the Zillerberget member) contains numerous parasequences which differ slightly from those of the upper part by being more heterolithic and rarely containing thick-bedded storm deposits (Figs 7A, 7B and 12D). In general, the entire lower part of the upper wedge is very heterolithic with a sandstone–shale ratio of *ca* 70:30 to 60:40 (Figs 7 and 12A), thus containing more sandstone than previously reported by Nagy (1970) who postulated that the unit is mostly mudstone-dominated. An aggradational parasequence stacking pattern is evident in the lower 400 m of the upper wedge (Fig. 7A).

**Interpretation.** The systematic stacking of UW 1 to UW 3 into coarsening-upward parasequences and the clear progradational stacking of PS 1 to PS 3 resemble stratigraphic trends commonly attributed to shoreline progradation in many other ancient storm-dominated and genetically linked shoreface–shelf systems (Aigner & Reineck, 1982; Van Wagoner *et al.*, 1990; Taylor & Lovell, 1995; Hampson & Storms, 2003; Helland-Hansen & Hampson, 2009). PS 4 to PS 7 display

a more aggradational to retrogradational stacking pattern, implying that PS 3 probably accumulated during maximum regression of the system (Figs 7B and 8). The lack of facies attributable to coastal plain or foreshore to upper shoreface deposition in any of the parasequences suggests that they accumulated under conditions persistently too deep for such deposits to accumulate. The dominance of wave-generated and storm-generated sedimentary structures in all of the facies associations (Fig. 14) supports a fully subaqueous origin of the parasequences. More exact palaeo-water depths are difficult to estimate because none of the investigated parasequences contains a complete facies succession going from offshore upward into foreshore and backshore deposits. Based on parasequence thicknesses recorded in this study (i.e. 10 to 30 m; Fig. 7), palaeo-water depth of some few tens of metres seems reasonable. This is consistent with inferred palaeo-water depths of five to a couple of hundred metres for HCS sandstones in other ancient shallow marine to offshore successions (e.g. Morsilli & Pomar, 2012; Jelby *et al.*, 2020).

Other causes for the lack of proximal nearshore to backshore facies may relate to wave ravinement during intervening transgressions (e.g. Cattaneo & Steel, 2003), or accretion during descending shoreline trajectory conditions preventing sufficient accommodation for proximal facies to be preserved (Helland-Hansen & Hampson, 2009). However, there are no indications supporting these interpretations. Alternatively, the parasequences may record the successive arrival and stacking of shore-detached offshore bars (Maher *et al.*, 2004). Offshore bars typically develop from storm-related and tidal reworking of relict shoreline and deltaic deposits in transgressed coastal areas (including isolated lowstand systems; e.g. Plint, 1988; Leva López *et al.*, 2016) or down-flank of major river distributaries (Olariu *et al.*, 2012), and they commonly exhibit other sedimentary characteristics than those documented in the present study (for example, various cliniform geometries, sharp erosive bases and cross-bedded sandstone beds; Leva López *et al.*, 2016). Considering the predominance of storm-wave-generated structures, the systematic parasequence stacking and their cumulative thickness (>100 m; Figs 7 and 8), and the abundance of sandstone in all of the facies associations (Fig. 14), the offshore bar model is the least favourable.

The heterolithic, yet sandstone-dominated, lower part of the upper wedge reflects

deposition on a shallow shelf as evident by the dominance of thin-bedded storm beds of UW 1 (Fig. 14). Across large parts of the shelf, even in the inferred deepest areas, the seafloor was apparently positioned above SWB. The occurrence of extensive storm-modulated sandstone sheets in ancient shelf successions has previously been linked to low shelf gradients and shallow water depths (Runkel *et al.*, 1998, 2007; Jelby *et al.*, 2020). Under such conditions, the effective SWB extends far offshore and thus controls tempestite deposition hundreds of kilometres seaward of the inferred palaeoshoreline. In middle shelf settings, internal waves forming on top of the bottom boundary layer during storms may interfere with the seafloor, potentially capable of generating hummocky bedforms (Morsilli & Pomar, 2012). This contrasts with classic tempestite facies models on distally deepening shelves where thin, normally graded turbidite beds occur below SWB (i.e. 'graded rhythmite'; e.g. Reineck & Singh, 1972; Dott & Bourgeois, 1982). The outer and deeper part of the shelf was an important sink which received large amounts of sand-grade sediment during accumulation of the upper wedge. The aggradational parasequence stacking trend in the lower part (i.e. the Zillerberget member; Fig. 7A) suggests that sediments aggraded as a storm-sculpted sheet across large parts of the shelf. When the shelf became shallow enough and the seafloor had aggraded to the effective SWB, PS 1 to PS 3 of the Schönrockfjellet member eventually prograded into and across the study area. These parasequences are strikingly similar to HCS sandstone-bearing subaqueous delta lobe units reported from the Mayaro Formation of the Columbus Basin, south-east Trinidad, by Bowman & Johnson (2014). The parasequences of the Mayaro Formation are characterized by a clear absence of foreshore and fluvial facies, in contrast to the classic shelf-shoreface-type parasequences described in many other ancient examples (e.g. Van Wagoner *et al.*, 1990; Taylor & Lovell, 1995; Hampson & Storms, 2003).

## DISCUSSION

### Comparison of stratigraphic architectures and storm-bed distribution

Cross & Lessenger (1997) attributed contrasting stratigraphic architectures between seaward-stepping and landward-stepping wedges to

variable sediment budgets strongly controlled by relative sea-level and shelf-water depths. Seaward-stepping sediment wedges, such as the lower wedge, generally form their own shallow platforms as they prograde across deep shelves (Fig. 18A; Cross & Lessenger, 1997). This implies that depositional profiles are generally relatively steep, and that a local relief may occur along the depositional dip of these wedges, promoting the generation of basinward-directed currents and enhancing the strength of offshore-directed downwelling flows following coastal setup (Fig. 18A).

The storm-influenced prodelta to delta front deposits (LW 4 'heterolithic sandstone deposits with scours'; Figs 14 and 15A) in the uppermost parasequence of the lower wedge contain frequent scours and other features pointing to erosion and subsequent deposition by hyperpycnal flows, combined flows and wave-modified turbidity currents (Figs 10E, 10G, 10I 13A and 14). This is in strong contrast to the underlying parasequences predominantly exhibiting isotropic HCS sandstone beds (Figs 15A and 18A). Scouring and channelization down-dip of distributary channels or in proximity to their subaqueous extensions have been described from ancient delta front successions elsewhere (e.g. Pattison *et al.*, 2007; Eide *et al.*, 2015).

In landward-stepping wedges, such as the middle wedge, abrupt bathymetric steps may develop on the seafloor across the platform break of retrogradationally stacked parasequences (Fig. 18B; Cross & Lessenger, 1997; Eide *et al.*, 2015). If a parasequence progrades into deeper water across the abrupt platform break of the preceding parasequence, scouring and channelization from bypassing turbidity currents may be expected (Eide *et al.*, 2015). In addition, the increased slope angles will potentially enhance the intensity of other shelf-crossing currents (for example, downwelling flows, storm surge flows, wave-modified gravity flows and/or tidal currents). Such local enhancement of unidirectional flows may thus explain the occurrence and stratigraphic distribution of scours and gutter casts (in MW 3; Figs 13D, 14 and 15C) and the associated combined-flow-generated structures including anisotropic HCS observed in the middle wedge (Fig. 18B).

The dominance of sedimentary structures generated by waves and storm-waves, and the contemporary lack of sedimentary structures formed by unidirectional currents in the upper wedge is enigmatic. The very heterolithic,

albeit sandstone-dominated, deposits of UW 1 ('thin-bedded storm deposits'; Fig 14), exhibit abundant wave-ripple cross-lamination, suggesting that the seafloor was mostly positioned above SWB and that even the deepest parts of shelf acted as a sand sink for prolonged periods of time. In order to enable sand transport across the shelf, sediments eroded from nearshore areas must have been kept in suspension by the oscillatory motion of fair-weather waves and in particular storm-waves (Fig. 17). On rare occasions, erosive storm-generated offshore-directed flows transported sand towards the distal part of the shelf (i.e. BT 8; Figs 9 and 12E). In general, the rate of accommodation creation (mainly governed by subsidence) was in equilibrium with the rate of sediment supply, resulting in aggradational stacking of parasequences in the lower part of the upper wedge (Fig. 7A). Thick-bedded isotropic HCS sandstone beds of UW 3 ('thick-bedded storm deposits') dominate the upper part of the wedge, reflecting progradation of more proximal facies belts (Figs 16, 17 and 18C). The amalgamated nature of these deposits indicates multiple periods of storm-wave reworking before final deposition and burial.

It seems unlikely that intense and recurrent storm-reworking erased nearly all combined-flow-related deposits of the upper wedge. Instead, the upper wedge must have formed under principally different hydrodynamic conditions than the two other wedges (compare Fig. 18A to 18C). A key observation is thus the sandstone-dominated, heterolithic nature of the inferred distal facies of the upper clastic wedge (UW 1 and UW 2; Figs 7, 12B and 14). This is in strong contrast with the lower wedge which displays a development from a thick, shale-dominated succession (LW 1 assigned to the Wimanfjellet Member; Figs 5A, 6A, 6D, 14 and 18A), representing offshore deposition below SWB, grading upward into sandstone-rich, shoreface to deltaic parasequences (i.e. the Kikutodden Member, LW 2 and LW 3; Figs 5A, 6A, 6E and 18A). As evidenced by the heterolithic deposits of the upper wedge (UW 1 and UW 2, for example, Figs 7 and 8), the shelf of the upper wedge must have been much shallower with a considerably larger proportion of the basin floor positioned above SWB compared to the lower wedge (Figs 17 and 18). Accommodation space was constantly filled by deposits of UW 1 ('thin-bedded storm deposits'; Fig. 14) and UW 2 ('thin to medium-bedded storm deposits'; Fig. 14), which repeatedly built up to FWFB before being

outpaced by subsidence (Figs 17 and 18). Eventually, the shelf became shallow enough to enable rapid progradation of PS 1 to PS 3 of the upper wedge (dominated by UW 3 'thick-bedded storm deposits'; Figs 7, 16, 17 and 18C). Alternatively, the inner shelf sheet of PS 1 to PS 3 was forced seaward as a result of relative sea-level fall (as is evident from the sharp base of PS 3; Figs 7B and 16A) governed by tectonically-induced uplift, eustatic sea-level fall, sudden decrease in subsidence rates, and/or increased sediment supply of sand. The relatively shallow shelf setting undoubtedly resulted in recurring and intense storm-wave reworking.

Tidal currents act as important transport agents on many modern epicontinental shelves, and various tidal-generated facies have been widely reported from ancient shelf systems (e.g. Olariu *et al.*, 2012; Leva López *et al.*, 2016). Tidal modulation of wave-dominated shorelines generally has the greatest effect at low-gradient shelves, but such settings are typically subjected to complex hydrodynamic processes inhibiting the development of conventional tidal sedimentary structures (Vakarelov *et al.*, 2012). Although no tidal indicators are present in the upper wedge, they do occur in the middle wedge (BT 16; Fig 9, see also Birkenmajer, 1966) and in a few sandstone beds of the lower wedge (Jelby *et al.*, 2020). Thus, if tidal currents ever played a role in sediment transport across the shelf of the upper wedge, intense storm-wave reworking would have overprinted any such tidal signature.

### **Stratigraphic responses to depositional processes and implications for storm-bed variability**

It is well-known that storm processes respond to changing shelf morphology and physiography (e.g. Mount, 1982; Brenchley *et al.*, 1986, 1993; Swift *et al.*, 1987; Midtgaard, 1996; Pérez-López, 2001; Runkel *et al.*, 2007; Basilici *et al.*, 2012b; Collins *et al.*, 2017; Jelby *et al.*, 2020). In the present study, scours, gutter casts and anisotropic HCS sandstone beds are shown to occur in several places in the lower and middle wedges (Figs 10, 11, 13, 18A and 18B; see also Nøttvedt & Kreisa, 1987; Jelby *et al.*, 2020). This is in contrast to what is observed in the upper wedge, which is dominated by wave and storm-wave generated structures in all of the facies associations (UW 1 to UW 3; Figs 14 and 16). Thus, it seems clear that storm-bed deposition is governed by multiple factors, including the overall shelf gradient,

local bathymetric variations, water depth, tidal currents, and local delivery systems such as delta fronts generating various offshore-directed currents, including downwelling and density-induced flows (Fig. 18; Jelby *et al.*, 2020). It also appears that the stratigraphic architecture of shoreface – inner shelf wedges is inherently related to several of these aspects (Fig. 18). In the seaward-stepping lower wedge (the Rurikfjellet Formation; Figs 2D, 3C, 5A, 6A and 6B), the development of, amongst others, scours, gutter casts and anisotropic HCS was predominantly favoured by downwelling currents, periodically of hyperpycnal character, deriving from an approaching delta system (as evidenced by LW 4; Figs 15A and 18A; Jelby *et al.*, 2020). Because the lower wedge built into deep waters, it had a comparatively steeper (but still low; see Jelby *et al.*, 2020) depositional dip than the middle and upper wedges (Figs 3C, 4B and 18A). This may locally have increased the role of gravity-driven currents.

In the landward-stepping middle wedge (the Dalkjegla Member; Figs 2D, 3A, 5B and 6B), anisotropic HCS formed in a middle shelf setting by strong shore-parallel or offshore-directed currents (as indicated by a large spread in palaeocurrent indicators), possibly associated with geostrophic flows. In addition, tidal currents have influenced storm-bed deposition, as evidenced by the local occurrence of shingled, compound hummocky beds (BT 16; Fig. 9). Thus, it may be speculated that the combination of storm-waves and tidal currents was responsible for the formation of the anisotropic HCS recorded in the middle wedge.

In landward-stepping wedges, abrupt bathymetric steps may have occurred across the platform break of successive retrogradationally stacked parasequences in middle to outer shelf settings (Fig. 18B; Cross & Lessenger, 1997; Eide *et al.*, 2015). These localized differences in bathymetric relief and dip angle may have promoted the generation and/or enhanced the intensity of offshore-directed currents, enabling currents to potentially scour into the underlying seafloor and deposit turbidites (as evidenced by the presence of BT 7 in the deposits of MW 2 and MW 3; for example, Fig. 11B) far offshore (Fig. 18B).

Based on the documented parasequence stacking, the upper wedge represents a seaward-stepping sediment-wedge (Figs 7 and 18C). However, considering the degree of storm-reworking and the abundance of isotropic HCS sandstone beds throughout the succession (Figs 7, 8, 12 and 16), it seems likely that the gradient was

comparatively small and the water shallower than the seaward-stepping lower wedge (Fig. 18). Ultimately, the result was a lowered SWB and intense storm-reworking.

## CONCLUSIONS

This study of storm-dominated shelf deposits within three siliciclastic sediment wedges in the Lower Cretaceous succession in Svalbard demonstrates how shelf morphology and physiography may influence storm-bed variability and the stratigraphic architecture of shelf–shoreface successions. The sedimentological and stratigraphic characteristics of the three wedges, all containing hummocky cross-stratified (HCS) sandstone storm deposits, are compared. The lower wedge, belonging to the Rurikfjellet Formation (Valanginian – lower Barremian) is seaward-stepping. The middle wedge, belonging to the Dalkjegla Member in the Aptian part of the Carolinefjellet Formation, is landward-stepping. The upper wedge, belong to the Schönrockfjellet and Zillerberget members in the middle Albian part of the Carolinefjellet Formation, is seaward-stepping.

- Sand-partitioning in seaward-stepping wedges building into deeper basins, such as the lower wedge, is controlled by comparably steeper depositional gradients (than those building into shallower water), the relative position of the storm-wave base (SWB) and the low efficiency of basinward-directed flows. Sand is predominantly trapped in the shoreface region above SWB, building its own subaqueous platform. Distal (and thus deeper) facies are predominantly characterized by a lack of sandstone, because the basin floor is primarily positioned below SWB. The occurrence of anisotropic HCS sandstone beds, scour-and-fill features (of hyperpycnal-flow origin) and wave-modified turbidite deposits in the uppermost part of the lower wedge were probably governed by a sudden change to prodelta and delta front environments associated with a forced regression and an approaching fluvio-deltaic system.

- The landward-stepping middle wedge may have developed localized bathymetric steps on the seafloor across the platform break of retrogradationally stacked parasequences. These rather abrupt steps with increased dip angles, promoted and enhanced the intensity of shelf-crossing combined flows and unidirectional currents, enabling scouring, bypass and locally also turbidite deposition. Tidal currents in combination with storm-

generated currents may also have influenced the development and migration of larger compound hummocky bedforms, as well as smaller bedforms preserved as anisotropic HCS.

- Thick, amalgamated units dominated by isotropic HCS sandstone beds in the upper wedge suggest deposition in a shallow, inner shelf setting prone to storm-wave reworking. The inferred distal facies are characterized by heterolithic, lenticular-bedded sandstone commonly exhibiting wave-ripple cross-lamination, suggesting that the basin floor was mostly positioned above SWB. This suggests comparatively lower gradients with an offshore-extended SWB position for the upper wedge, allowing for intense storm-reworking of the shelf which hampered the preservation of facies deposited by other processes.

- Collectively, this study demonstrates that storm-depositional processes and corresponding storm-bed facies architectures and variability in many cases are influenced by changing shelf morphology and basin physiography, including the effects of relative sea-level change, storm and tidal interactions, and the proximity to fluvial feeder systems.

## ACKNOWLEDGEMENTS

The authors are grateful to the sponsors of the LoCrA consortium (Lower Cretaceous Basin Studies in The Arctic; <https://wp.uu.uis.no/locra>) for providing us financial support to carry out fieldwork. Ivar Midtkandal is thanked for companionship in the field and for reading through an earlier version of the manuscript. Linda Cecilia Haaland and Peter Alsen are acknowledged for their assistance and company in the field. Harmon Maher and one anonymous reviewer are thanked for their constructive comments on an earlier version of the manuscript. Journal reviews by Gary Hampson, José Miguel Molina, Valentina Rossi and one anonymous reviewer are highly appreciated. We also thank Sergio Longhitano for his comments to the revised version of the manuscript. SAG and SO received support from the ARCEX project which is funded by the Research Council of Norway (grant number 228107).

## DATA AVAILABILITY STATEMENT

The data that support the findings of this study are available from the corresponding author upon reasonable request.

## REFERENCES

- Aigner, T. and Reineck, H.-E. (1982) Proximality trends in modern storm sands from the Helegoland Bight (North Sea) and their implications for basin analysis. *Senckenb. Marit.*, **14**, 183–215.
- Amos, C.L., Li, M.Z., Chiocci, F.L., La Monica, G.B., Cappucci, S., King, E.H. and Corbani, F. (2003) Origin of shore-normal channels from the shoreface of Sable Island, Canada. *J. Geophys. Res.*, **108**, 1–16.
- Århus, N. (1991) Dinoflagellate cyst stratigraphy of some Aptian and Albian sections from North Greenland, southeastern Spitsbergen and the Barents Sea. *Cretaceous Res.*, **12**, 209–225.
- Arnott, R.W.C. (1993) Quasi-planar-laminated sandstone beds of the Lower Cretaceous Bootlegger Member, Northcentral Montana: evidence of combined-flow sedimentation. *J. Sed. Petrol.*, **63**, 488–494.
- Arnott, R.W.C. and Southard, J.B. (1990) Exploratory flow-duct experiments on combined-flow bed configurations, and some implications for interpreting storm-event stratification. *J. Sed. Petrol.*, **60**, 211–219.
- Basilici, G., Vieira de Luca, P.H. and Poiré, D.G. (2012a) Hummocky cross-stratification-like structures and combined-flow ripples in the Punta Negra Formation (Lower-Middle Devonian, Argentine Precordillera): A turbiditic deep-water or storm-dominated prodelta inner-shelf system? *Sed. Geol.*, **267–268**, 73–92.
- Basilici, G., de Luca, P.H.V. and Oliveira, P. (2012b) A depositional model for a wave-dominated open-coast tidal flat, based on analyses of the Cambrian-Ordovician Lagarto and Palmares formations, north-eastern Brazil. *Sedimentology*, **59**, 1613–1639.
- Bhattacharya, J.P. and MacEachern, J.A. (2009) Hyperpycnal rivers and prodeltaic shelves in the Cretaceous Seaway of North America. *J. Sed. Res.*, **79**, 184–209.
- Birkenmajer, K. (1966) Lower cretaceous tidal deposits of central vest Spitsbergen. *Norsk Polarinst. Årbok*, **1964**, 73–85.
- Bourgeois, J. (1980) A transgressive shelf sequence exhibiting hummocky stratification: The Cape Sebastian Sandstone (Upper Cretaceous), southwestern Oregon. *J. Sed. Petrol.*, **50**, 681–702.
- Bowman, A.P. and Johnson, H.D. (2014) Storm-dominated shelf-edge delta successions in a high accommodation setting: The palaeo-Orinoco Delta (Mayaro Formation), Columbus Basin, South-East Trinidad. *Sedimentology*, **61**, 792–835.
- Brenchley, P.J., Romano, M. and Gutiérrez-Marco, J.C. (1986) Proximal and distal hummocky cross-stratified facies on a wide Ordovician shelf in Iberia. In: *Shelf Sands and Sandstones* (Eds Knight, R.J. and McLean, J.R.), *Can. Soc. Petrol. Geol. Mem.*, **2**, 241–255.
- Brenchley, P.J., Pickerill, R.K. and Stromberg, S.G. (1993) The role of wave reworking in the architecture of storm sandstone facies, Bell Island Group (Lower Ordovician), eastern Newfoundland. *Sedimentology*, **40**, 359–382.
- Campbell, M.D. and Campbell, M.D. (2018) Paleoenvironmental implications of selected siderite zones in the Upper Atoka Formation, Arkoma Basin, Oklahoma-Arkansas: a look back and current views on siderite genesis in a sedimentary Environment. *Int. J. Earth Sci. Geol.*, **1**, 6–40.
- Carvajal, C. and Steel, R.J. (2009) Shelf-edge architecture and bypass of sand to deep water: influence of shelf-edge processes, sea level, and sediment supply. *J. Sed. Res.*, **79**, 652–672.
- Cattaneo, A. and Steel, R.J. (2003) Transgressive deposits: a review of their variability. *Earth-Sci. Rev.*, **62**, 187–228.
- Cheel, R.J. and Leckie, D.A. (1993) Hummocky Cross-stratification. *Sed. Rev.*, **1**, 103–122.
- Clifton, H.E. (1976) Wave-formed sedimentary structures – A conceptual model. In: *Beach and Nearshore Sedimentation* (Eds Davis, R.A. and Ethington, R.L.), *SEPM Special Publication*, **24**, 126–148.
- Collins, D.S., Johnson, H.D., Allison, P.A., Guilpain, P. and Damit, A.R. (2017) Coupled ‘storm-flood’ depositional model: Application to the Miocene-Modern Baram Delta Province, north-west Borneo. *Sedimentology*, **64**, 1203–1235.
- Corfu, F., Polteau, S., Planke, S., Faleide, J.I., Svensen, H., Zayoncheck, A. and Stolbov, N. (2013) U-Pb geochronology of Cretaceous magmatism on Svalbard and Franz Josef Land, Barents Sea Large Igneous Province. *Geol. Mag.*, **150**, 1127–1135.
- Cross, T.A. and Lessenger, M.A. (1997) Correlation strategies for clastic wedges. In: *Innovative applications of petroleum technology in the Rocky Mountain Area* (Eds Coalson, E.B., Osmond, J.C. and Williams, E.T.), pp. 183–203. Rocky Mountain Association Geologist, Denver, CO.
- Dott, R.J. and Bourgeois, J. (1982) Hummocky stratification: Significance of its variable bedding sequences. *Geol. Soc. Am. Bull.*, **93**, 663–680.
- Duke, W.L. (1985) Hummocky cross stratification, tropical hurricanes, and intense winter storms. *Sedimentology*, **32**, 167–194.
- Duke, W.L. (1990) Geostrophic circulation or shallow marine turbidity currents? The dilemma of paleoflow patterns in storm-influenced prograding shoreline systems. *J. Sed. Petrol.*, **60**, 870–883.
- Duke, W.L., Arnott, R.W.C. and Cheel, R.J. (1991) Shelf sandstones and hummocky cross-stratification: New insight on a stormy debate. *Geology*, **19**, 625–628.
- Dumas, S. and Arnott, R.W.C. (2006) Origin of hummocky and swaley crossstratification—The controlling influence of unidirectional current strength and aggradation rate. *Geology*, **34**, 1073–1076.
- Dumas, S., Arnott, R.W.C. and Southard, J.B. (2005) Experiments on oscillatory flow and combined-flow bed forms; implications for interpreting parts of the shallow-marine sedimentary record. *J. Sed. Res.*, **75**, 501–513.
- Dypvik, H., Nagy, J., Eikeland, T.A., Backe-Owe, K., Andresen, A., Haremo, P., Bjerke, T., Johansen, H. and Elverhøi, A. (1991a) The Janusfjellet Subgroup (Bathonian to Hauterivian) on central Spitsbergen: a revised lithostratigraphy. *Polar Res.*, **9**, 21–43.
- Dypvik, H., Nagy, J., Eikeland, T.A., Backer-Owe, K. and Johansen, H. (1991b) Depositional conditions of the Bathonian to Hauterivian Janusfjellet Subgroup, Spitsbergen. *Sed. Geol.*, **72**, 55–78.
- Dypvik, H., Hakansson, E. and Heinberg, C. (2002) Jurassic and Cretaceous palaeogeography and stratigraphic comparisons in the North Greenland-Svalbard region. *Polar Res.*, **21**, 91–108.
- Eide, C.H., Howell, J.A. and Buckley, S.J. (2015) Sedimentology and reservoir properties of tabular and erosive offshore transition deposits in wave-dominated, shallow-marine strata: Book Cliffs, USA. *Petrol. Geosci.*, **21**, 55–73.
- Gjelberg, J., Steel, R.J. (1995) Helvetiafjellet Formation (Barremian-Aptian), Spitsbergen: characteristics of a transgressive succession. In: *Sequence Stratigraphy on the Northwest European margin* (Eds Steel, R.J.), pp. 571–593. Elsevier, Amsterdam.

- Grantz, A., Hart, P.E. and Childers, V.A.** (2011). Geology and tectonic development of the Amerasia and Canada Basins, Arctic Ocean. In: *Arctic Petroleum Geology* (Eds Spencer, A.M., Gautier, D., Stoupakova, A., Embry, A. and Sorensen, K.), *Geol. Soc., London Mem.*, **35**, 771–799.
- Grundvåg, S.-A. and Olausen, S.** (2017) Sedimentology of the Lower Cretaceous at Kikutodden and Keilhaufjellet, southern Spitsbergen: implications for an onshore offshore link. *Polar Res.*, **36**(1), 1302124.
- Grundvåg, S.-A., Johannessen, E.P., Helland-Hansen, W. and Plink-Björklund, P.** (2014) Depositional architecture and evolution of progradationally stacked lobe complexes in the Eocene Central Basin of Spitsbergen. *Sedimentology*, **61**, 535–569.
- Grundvåg, S.-A., Olausen, S., Midtkandal, I. and Śliwińska, K.K.** (2015) The architecture of a regressive wedge in an overall transgressive shelf sequence: the Schönrockfjellet member of the Carolinefjellet Formation, southeastern Spitsbergen. In: *NGF Abstracts and Proceedings*, vol. 1 (Eds Nakrem, H.A. and Husås, A.M.), p. 35, Norsk Geologisk Forening, Trondheim.
- Grundvåg, S.-A., Marin, D., Kairanov, B., Śliwińska, K.K., Nøhr-Hansen, H., Jelby, M.E., Escalona, A. and Olausen, S.** (2017) The Lower Cretaceous succession of the northwestern Barents Shelf: Onshore and offshore correlations. *Mar. Petrol. Geol.*, **86**, 834–857.
- Grundvåg, S.A., Jelby, M.E., Śliwińska, K.K., Nøhr-Hansen, H., Aadland, T., Sandvik, S.E., Tennvassås, I., Engen, T. and Olausen, S.** (2019) Sedimentology and palynology of the Lower Cretaceous succession of central Spitsbergen: integration of subsurface and outcrop data. *Norwegian J. Geol.*, **99**, 253–284.
- Hampson, G.J. and Storms, J.E.A.** (2003) Geomorphological and sequence stratigraphic variability in wave-dominated, shoreface-shelf parasequences. *Sedimentology*, **50**, 667–701.
- Harms, J.C., Southard, J.B., Spearing, D.R. and Walker, R.G.** (1975) Depositional environments as interpreted from primary sedimentary structures and stratification sequences. SEPM Course Notes No. 2, 161 pp.
- Hay, W.W.** (2009) Cretaceous Oceans and Ocean Modeling. In: *Cretaceous Oceanic Red Beds: Stratigraphy, Composition, Origins, and Paleocceanographic and Paleoclimatic Significance* (Eds Hu, X., Wang, C., Scott, R.W., Wagneich, M. and Jansa, L.), *SEPM Spec. Publ.*, **91**, 243–271.
- Helland-Hansen, W. and Hampson, G.** (2009) Trajectory analysis: concepts and applications. *Basin Res.*, **21**, 454–483.
- Hurum, J.H., Roberts, A.J., Dyke, G.J., Grundvåg, S.-A., Nakrem, H.A., Midtkandal, I., Śliwińska, K.K. and Olausen, S.** (2016) Bird or maniraptoran dinosaur? A femur from the Albian strata of Spitsbergen. *Palaeontol. Polonica.*, **67**, 137–147.
- Jelby, M.E., Grundvåg, S.-A., Helland-Hansen, W., Olausen, S. and Stemmerik, L.** (2020) Tempestite facies variability and storm-depositional processes across a wide ramp: Towards a polygenetic model for hummocky cross-stratification. *Sedimentology*, **67**, 742–781.
- Johnson, H.D.** (1977) Shallow marine sand bar sequence: an example from the Late Precambrian of North Norway. *Sedimentology*, **24**, 245–270.
- Lamb, M.P., Myrow, P.M., Lukens, C. and Houck, K.** (2008) Deposits from wave-influenced turbidity currents: Pennsylvanian Minturn Formation, Colorado, U.S.A. *J. Sed. Res.*, **78**, 480–498.
- Leckie, D.A. and Krystinik, L.F.** (1989) Is there evidence for geostrophic current preserved in the sedimentary record of inner to middle-shelf deposits? *J. Sed. Petrol.*, **59**, 862–870.
- Leckie, D.A. and Walker, R.G.** (1982) Storm- and tide-dominated shorelines in Cretaceous Moosebar–lower Gates interval—Outcrop equivalents of deep basin gas trap in western Canada. *AAPG Bull.*, **66**, 138–157.
- Leva López, J., Rossi, V.M., Olariu, C. and Steel, R.J.** (2016) Architecture and recognition criteria of ancient shelf ridges; an example from Campanian Almond Formation in Hanna Basin, USA. *Sedimentology*, **63**, 1651–1676.
- Macquaker, J.H.S., Bentley, S.J. and Bohacs, K.M.** (2010) Wave-enhanced sediment-gravity flows and mud dispersal across continental shelves: reappraising sediment transport processes operating in ancient mudstone successions. *Geology*, **38**, 947–950.
- Maher, H.D.** (2001) Manifestations of the Cretaceous high arctic large igneous province in Svalbard. *J. Geol.*, **109**, 91–104.
- Maher, H.D. and Shuster, R.** (2007) Attributes of a Cretaceous storm bed from Spitsbergen, Norway. Poster presented at GSA 2007 Annual Meeting, Denver, USA, 28–31 October.
- Maher, H.D., Hays, T., Shuster, R. and Mutrux, J.** (2004) Petrography of the Lower Cretaceous sandstones of Spitsbergen. *Polar Res.*, **23**, 147–165.
- Martel, A.T. and Gibling, M.R.** (1994) Combined-flow generation of sole structures, including recurved groove casts, associated with Lower Carboniferous lacustrine storm deposits in Nova Scotia, Canada. *J. Sed. Res.*, **64**, 508–517.
- Marin, D., Escalona, A., Śliwińska, K.K., Nøhr-Hansen, H. and Mordasova, A.** (2016) Sequence stratigraphy and lateral variability of Lower Cretaceous clinofolds in the SW Barents Sea. *AAPG Bull.*, **101**, 1487–1517.
- Midtgaard, H.H.** (1996) Inner-shelf to lower-shoreface hummocky sandstone bodies with evidence for geostrophic influenced combined flow, Lower Cretaceous, West Greenland. *J. Sed. Res.*, **66**, 343–353.
- Midtkandal, I. and Nystuen, J.P.** (2009) Depositional architecture of a low-gradient ramp shelf in an epicontinental sea: the Lower Cretaceous of Svalbard. *Basin Res.*, **21**, 655–675.
- Midtkandal, I., Svensen, H., Planke, S., Corfu, F., Polteau, S., Torsvik, T., Faleide, J.I., Grundvåg, S.-A., Selnes, H. and Olausen, S.** (2016) The Aptian oceanic anoxic event (OAE1a) in Svalbard and the age of the Barremian-Aptian boundary. *Palaeogeogr. Palaeoclimatol. Palaeoecol.*, **463**, 126–135.
- Midtkandal, I., Faleide, J.I., Faleide, T.S., Serck, C.S., Planke, S., Corseri, R., Dimitriou, M. and Nystuen, J.P.** (2019) Lower Cretaceous Barents Sea strata: epicontinental basin configuration, timing, correlation and depositional dynamics. *Geol. Mag.*, **157**(3), 458–476.
- Morsilli, M. and Pomar, L.** (2012) Internal waves vs. surface storm waves: a review on the origin of hummocky cross-stratification. *Terra Nova*, **24**, 273–282.
- Mount, J.F.** (1982) Storm-surge-ebb origin of hummocky cross-stratified units of the Andrews Mountain Member, Campito Formation (Lower Cambrian), White-Inyo Mountains, eastern California. *J. Sed. Res.*, **52**, 941–958.
- Mulder, T., Syvitski, J.P.M., Migeon, S., Faugères, J.-C. and Savoye, B.** (2003) Marine hyperpycnal flows: initiation, behavior and related deposits, A review. *Mar. Petrol. Geol.*, **20**, 861–882.

- Muttrux, J., Maher, H., Shuster, R. and Hays, T.** (2008) Iron ooid beds of the Carlinefjellet Formation, Spitsbergen, Norway. *Polar Res.*, **27**, 28–43.
- Myrow, P.M.** (1992a) Pot and gutter casts from the Chapel Island Formation, Southeast Newfoundland. *J. Sed. Petrol.*, **62**, 992–1007.
- Myrow, P.M.** (1992b) Bypass-zone tempestite facies model and proximity trends for an ancient muddy shoreline and shelf. *J. Sed. Petrol.*, **62**, 99–115.
- Myrow, P.M. and Southard, J.B.** (1996) Tempestite deposition. *J. Sed. Res.*, **66**, 875–887.
- Myrow, P.M., Woodward, F. and Goodge, J.W.** (2002) Wave-modified turbidites: Combined-flow shoreline and shelf deposits, Cambrian, Antarctica. *J. Sed. Res.*, **72**, 641–656.
- Mørk, A., Dallmann, W.K., Dypvik, H., Johannesen, E.P., Larssen, G.B., Nagy, J., Nøttvedt, A., Olausen, S., Pchelina, T.M. and Worsley, D.** (1999) Mesozoic lithostratigraphy. In: *Lithostratigraphic lexicon of Svalbard. Review and recommendations for nomenclature use. Upper Palaeozoic to Quaternary bedrock* (Ed. Dallmann, W.K.), pp. 127–214. Norsk Polarinstitut, Tromsø.
- Nagy, J.** (1970) Ammonite faunas and stratigraphy of Lower Cretaceous (Albian) rocks in southern Spitsbergen. *Nor Polarinst Skr.*, **152**, 1–58.
- Nemec, W., Steel, R.J., Gjelberg, J., Collinson, J.D., Prestholm, E. and Øxnevad, I.E.** (1988) Anatomy of collapsed and re-established delta front in Lower Cretaceous of Eastern Spitsbergen: gravitational sliding and sedimentation processes. *AAPG Bull.*, **72**, 454–476.
- Nøttvedt, A. and Kreisa, R.** (1987) Model for the combined-flow origin of hummocky cross-stratification. *Geology*, **15**, 357–361.
- Olariu, C., Steel, R.J., Dalrymple, R.W. and Gingras, M.K.** (2012) Tidal dunes versus tidal bars: The sedimentological and architectural characteristics of compound dunes in a tidal seaway, the lower Baronia Sandstone (Lower Eocene), Ager Basin, Spain. *Sed. Geol.*, **279**, 134–155.
- Olausen, S., Larssen, G.B., Helland-Hansen, W., Johannesen, E.P., Nøttvedt, A., Riis, F., Rismyhr, B., Smelror, M. and Worsley, D.** (2018) Mesozoic strata of Kong Karls Land, Svalbard, Norway; a link to the northern Barents Sea basins and platforms. *Norwegian J. Geol.*, **98**, 1–69.
- Parsons, J.D., Bush, J.W. and Syvitski, J.P.M.** (2001) Hyperpycnal plume formation from riverine outflows with small sediment concentrations. *Sedimentology*, **48**, 465–478.
- Pattison, S.A.J., Ainsworth, R.B. and Hoffman, T.A.** (2007) Evidence of across-shelf transport of fine-grained sediments: turbidite-filled shelf channels in the Campanian Aberdeen Member, Book Cliffs, Utah, USA. *Sedimentology*, **54**, 1033–1063.
- Peng, Y., Steel, R.J. and Olariu, C.** (2016) Transition from storm wave-dominated outer shelf to gullied upper slope: The mid-Pliocene Orinoco shelf margin, South Trinidad. *Sedimentology*, **64**, 1511–1539.
- Pérez-López, A.** (2001) Significance of pot and gutter casts in a Middle Triassic carbonate platform, Betic Cordillera, southern Spain. *Sedimentology*, **48**, 1371–1388.
- Plint, A.G.** (1988) Sharp-based shoreface sequences and “off-shore bars” in the Cardium Formation of Alberta: their relationship to relative changes in sea-level. In: *Sea-level change—an integrated approach* (Eds Wilgus, C.K., Hastings, B.S., Ross, C.A., Posamentier, H., Van Wagoner, J. and Kendall, and C.G. St. C.). *SEPM Spec. Publ.*, **42**, 357–370.
- Plint, A.G.** (2014) Mud dispersal across a Cretaceous prodelta: storm-generated, wave-enhanced sediment gravity flows inferred from mudstone microtexture and microfacies. *Sedimentology*, **61**, 609–647.
- Ponce, J.J., Olivero, E.B. and Martinioni, D.R.** (2008) Upper Oligocene-Miocene clinoforms of the foreland Austral Basin of Tierra del Fuego, Argentina: Stratigraphy, depositional sequences and architecture of the foredeep deposits. *J. S. Am. Earth Sci.*, **26**, 36–54.
- Quin, J.G.** (2011) Is most hummocky cross stratification formed by large-scale ripples? *Sedimentology*, **58**, 1414–1433.
- Reineck, H.E. and Singh, I.B.** (1972) Genesis of laminated sand and graded rhytmities in storm-sand layers of shelf mud. *Sedimentology*, **18**, 123–128.
- Runkel, A.C., McKay, R.M. and Palmer, A.R.** (1998) Origin of a classic cratonic sheet sandstone: Stratigraphy across the Sauk II–Sauk III boundary in the Upper Mississippi Valley. *GSA Bull.*, **110**, 188–210.
- Runkel, A.C., Miller, J.F., McKay, R.M., Palmer, A.R. and Taylor, J.F.** (2007) High-resolution sequence stratigraphy of lower Paleozoic sheet sandstones in central North America: The role of special conditions of cratonic interiors in development of stratal architecture. *GSA Bull.*, **119**, 860–881.
- Senger, K., Tveranger, J., Ogata, K., Braathen, A. and Planke, S.** (2014) Late Mesozoic magmatism in Svalbard: a review. *Earth-Sci. Rev.*, **139**, 123–144.
- Shephard, G.E., Müller, R.D. and Seton, M.** (2013) The tectonic evolution of the Arctic since Pangea breakup: Integrating constraints from surface geology and geophysics with mantle structure. *Earth-Sci. Rev.*, **124**, 148–183.
- Shipilov, E.V.** (2008) Generations of Spreading Basins and Stages of Breakdown of Wegener’s Pangea in the Geodynamic Evolution of the Arctic Ocean. *Geotectonics*, **42**, 105–124.
- Śliwińska, K.K., Jelby, M.E., Grundvåg, S.-A., Nøhr-Hansen, H. and Olausen, S.** (2020) Dinocyst stratigraphy of the Valanginian–Aptian Rurikfjellet and Helvetiafjellet formations on Spitsbergen, Arctic Norway. *Geol. Mag.*, 1–22. <https://doi.org/10.1017/S0016756819001249>
- Southard, J.B., Lambie, J.M., Federico, D.C., Pile, H.T. and Weidman, C.R.** (1990) Experiments on bed configurations in fine sands under bidirectional purely oscillatory flow, and the origin of hummocky cross-stratification. *J. Sed. Petrol.*, **60**, 1–17.
- Steel, R.J. and Worsley, D.** (1984) Svalbard’s post-Caledonian strata – an atlas of sedimentational patterns and palaeogeographic evolution. In: *Petroleum Geology of the North European Margin* (Ed A.M. Spencer). pp. 109–135. Norwegian Petroleum Society, Graham and Trotman Ltd, London.
- Swift, D.J.P., Hudelson, P.M., Brenner, R.L. and Thompson, P.** (1987) Shelf construction in a foreland basin: storm beds, shelf sandbodies, and shelf-slope depositional sequences in the Upper Cretaceous Mesaverde Group, Book Cliffs, Utah. *Sedimentology*, **34**, 423–457.
- Taylor, A.M. and Goldring, R.** (1993) Description and analysis of bioturbation and ichnofabric. *J. Geol. Soc. London*, **150**, 141–148.
- Taylor, D.R. and Lovell, R.W.W.** (1995) High-Frequency Sequence Stratigraphy and Paleogeography of the Kenilworth Member, Blackhawk Formation, Book Cliffs, Utah, U.S.A. *AAPG Mem.*, **64**, 257–275.
- Tinterri, R.** (2011) Combined flow sedimentary structures and the genetic link between sigmoidal- and hummocky cross stratification. *GeoActa*, **10**, 43–85.

- Torsvik, T.H., Van der Voo, R., Preeden, U., Niocaill, C.M., Steinberger, B., Doubrovine, P.V., van Hinsbergen, D.J.J., Domeier, M., Gaina, C., Tohver, E., Meert, J.G., McCausland, P.J.A. and Cocks, L.R.M.** (2012) Phanerozoic polar wander, palaeogeography and dynamics. *Earth-Sci. Rev.*, **114**, 325–368.
- Vakarelov, B.K., Ainsworth, R.B. and MacEachern, J.A.** (2012) Recognition of wave-dominated, tide-influenced shoreline systems in the rock record: Variations from a microtidal shoreline model. *Sed. Geol.*, **279**, 23–41.
- Van Wagoner, J.C., Mitchum, R.M., Campion, K.M. and Rahmanian, V.D.** (1990) Siliciclastic sequence stratigraphy in well logs, cores and outcrops. *AAPG Meth. Explor. Ser.*, **7**, 55.
- Varban, B.L. and Plint, G.** (2008) Palaeoenvironments, palaeogeography, and physiography of a large, shallow, muddy ramp: Late Cenomanian-Turonian Kaskapau Formation, Western Canada foreland basin. *Sedimentology*, **55**, 201–233.
- Walker, R.G.** (1984) Shelf and shallow marine sands. In: *Facies Models* (Ed. **Walker, R.G.**). *Geological Association of Canada, Geoscience Canada Reprint Series*, **1**, 2nd edn, 141–170.
- Wilson, R.D. and Schieber, J.** (2015) Sedimentary facies and depositional environment of the Middle Devonian Genesee Formation of New York, U.S.A. *J. Sed. Res.*, **85**, 1393–1415.

*Manuscript received 3 October 2019; revision 8 July 2020; revision accepted 20 July 2020*